RESEARCH ARTICLE

Key Points:
- Iron fertilization of blooms downstream of Southern Ocean islands studied with Lagrangian modeling
- Ocean areas fertilized by simulated iron transport overlap with observed spatial extent of blooms
- Inter-annual variability of iron input explains blooms at Crozet but not Kerguelen or South Georgia

Supporting Information:
- Supporting Information S1

Correspondence to:
J. Robinson,
josie.robinson@noc.soton.ac.uk

A tale of three islands: Downstream natural iron fertilization in the Southern Ocean

J. Robinson[1,2], E. E. Popova[1], M. A. Srokosz[1], and A. Yool[1]

[1]National Oceanography Centre, University of Southampton, Southampton, UK, [2]Ocean and Earth Science, University of Southampton, Southampton, UK

Abstract Iron limitation of primary productivity prevails across much of the Southern Ocean but there are exceptions; in particular, the phytoplankton blooms associated with the Kerguelen Plateau, Crozet Islands, and South Georgia. These blooms occur annually, fertilized by iron and nutrient-rich shelf waters that are transported downstream from the islands. Here we use a high-resolution (1/12°) ocean general circulation model and Lagrangian particle tracking to investigate whether inter-annual variability in the potential lateral advection of iron could explain the inter-annual variability in the spatial extent of the blooms. Comparison with ocean color data, 1998–2007, suggests that iron fertilization via advection can explain the extent of each island's annual bloom, but only the inter-annual variability of the Crozet bloom. The area that could potentially be fertilized by iron from Kerguelen was much larger than the bloom, suggesting that there is another primary limiting factor, potentially silicate, that controls the inter-annual variability of bloom spatial extent. For South Georgia, there are differences in the year-to-year timing of advection and consequently fertilization, but no clear explanation of the inter-annual variability observed in the bloom's spatial extent has been identified. The model results suggest that the Kerguelen and Crozet blooms are terminated by nutrient exhaustion, probably iron and or silicate, whereas the deepening of the mixed layer in winter terminates the South Georgia bloom. Therefore, iron fertilization via lateral advection alone can explain the annual variability of the Crozet bloom, but not fully that of the Kerguelen and South Georgia blooms.

1. Introduction

It is now generally accepted that iron, in conjunction with light, is a major limiting factor of primary production in the Southern Ocean, indirectly controlling the biological pump and drawdown of carbon dioxide from the atmosphere [*Takahashi et al.*, 2009; *Blain et al.*, 2007; *Boyd et al.*, 2007; *de Baar et al.*, 1995; *Martin*, 1990; *Martin et al.*, 1990]. However, there are exceptions to the high-nutrient, low-chlorophyll conditions that prevail across most of the Southern Ocean. Large phytoplankton blooms are observed downstream of continental shelf and land mass [*Blain et al.*, 2007; *Pollard et al.*, 2007; *Korb et al.*, 2008], where iron is suggested to be supplied to surface waters predominately from ocean sediments [*Bakker et al.*, 2007; *Tyrrell et al.*, 2005; *Thomalla et al.*, 2011]. In order to understand these important high-productivity regions, we need to characterize the time scales and mechanisms that transport iron to where primary production occurs [*Boyd et al.*, 2012a, 2012b; *d'Ovidio et al.*, 2015; *Wadley et al.*, 2014]. Here we focus on three Southern Ocean islands groups, the Kerguelen Plateau, Crozet Islands, and South Georgia and Shag Rocks, outlined by black boxes in Figure 1a, specifically looking at the role of advection in determining the spatial extent of the downstream blooms.

Iron supply in the Southern Ocean comes from a variety of different sources including: aeolian input, brine rejection and drainage from sea ice, sediments, entrainment from the deep ocean via winter mixing, Ekman pumping, and upwelling at ocean fronts, and it is also constantly resupplied via rapid recycling of organic material [*Boyd and Ellwood*, 2010; *Gille et al.*, 2014; *Graham et al.*, 2015; *Korb et al.*, 2008; *Schallenberg et al.*, 2016; *Tagliabue et al.*, 2014]. A recent study by *Graham et al.* [2015] suggests that coastlines, continental and island, are key sources of iron to the Southern Ocean, and also provides a comprehensive description of the behavior of iron in sediment pore waters and the mechanisms behind its flux into over-lying bottom water. Another source, recently found to be relevant to the Kerguelen Plateau, is riverine input associated with snowmelt. This source is important during spring, as there is increased rainfall and run-off, whereas freezing conditions during the winter inhibit this iron supply [*van der Merwe et al.*, 2015]. In
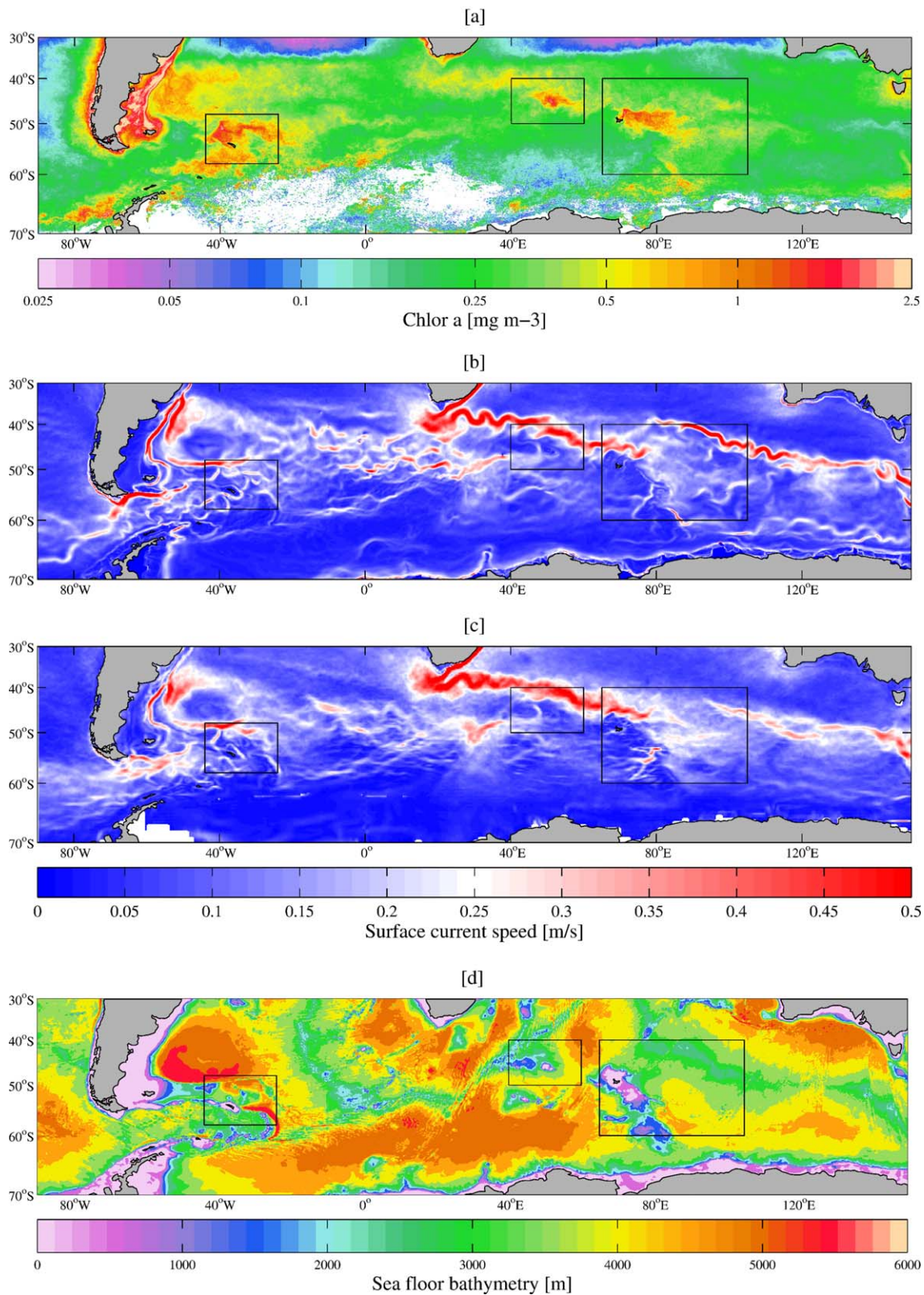
Figure 1. A Southern Ocean overview of satellite ocean color, satellite and modeled surface current speed, and the bathymetry in the model. (a) Decadal average, 1998–2007, of the chlorophyll *a* concentration (mg m^{-3}) in the month of November. (b and c) The decadal averages (1998–2007) of surface current speed (m^{-1}), from the NEMO model, at 1/12°, and the Aviso data, at 1/4° resolution, respectively. (d) The Southern Ocean bathymetry within the NEMO 1/12° model, contours are in meters below the sea surface. Black boxes denote the study areas: South Georgia, left; Crozet Islands, middle; Kerguelen, right.
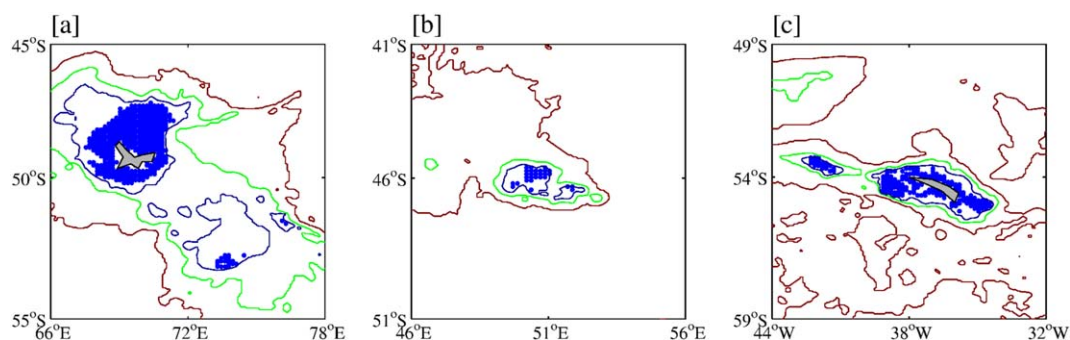
Figure 2. The starting positions of the Lagrangian particles around the islands. Particles are placed over shallow bathymetry (<180 m), around (a) Kerguelen and Heard Island, (b) Crozet Islands, and (c) South Georgia and Shag Rocks. In plots 2a and 2c, only every other particle is plotted for clarity. The plot also includes contours of 500 m (dark blue), 1500 m (green), and 3000 m (red) isobaths. Note that the axis for each plot is not consistent.

this paper, we focus on the potential for iron fertilization from island sources, primarily from sediments and runoff.

As iron is released from island sediments, internal waves and turbulence mix the iron up into surface waters which then fuels phytoplankton production [*Bowie et al.*, 2015; *Boyd*, 2007; *Korb et al.*, 2008; *Park et al.*, 2008a, 2008b]. Iron that is not immediately utilized by biota or scavenged from the water column can be transported downstream of its source via lateral advection within the local circulation and also by stirring within mesoscale features [*Abraham et al.*, 2000; *d'Ovidio et al.*, 2015]. As it advects, iron can undergo many processes and transformations as part of the complex iron cycle, which can alter both the transport and bioavailability of iron. For instance, iron can be diluted by physical mixing, it can be kept in circulation by iron-binding ligands, or there can be luxury uptake of the iron by biota and hence "internal advection" [*Mongin et al.*, 2008]. In various forms, iron can be lost from the surface by sinking or it can be retained in the surface water and then remineralized downstream of the original source and supply a new area with iron [*Boyd et al.*, 2000; *Boyd*, 2007].

In order to test the hypothesis that inter-annual variability observed in the spatial extent of downstream island blooms could be explained by horizontal advection, the details of the iron cycle are not considered here. In this paper, the term "iron advection" refers to any iron from island sources in a form that can be laterally transported, via either advection or stirring, and is also bioavailable at the bloom site, hence what is demonstrated in this paper is the potential for iron fertilization. To diagnose the advection around each island, Lagrangian particles were released within velocity fields from the NEMO (Nucleus for European Modelling of the Ocean) 1/12° ocean general circulation model, a resolution high enough to resolve eddies and small-scale circulation patterns around the islands. In the analysis, the Lagrangian trajectories, representing water mass potentially fertilized with iron, are compared against the observed bloom areas in the satellite data. Additionally, the possible causes for bloom termination will be considered for each island, utilizing the model diagnostics and also World Ocean Atlas nutrient data.

2. Methodology

In order to assess the impact of iron that could potentially be advected downstream of Southern Ocean islands, satellite-derived data (chlorophyll *a* concentrations and sea surface currents) were compared with Lagrangian particle trajectories within velocity output from the NEMO 1/12° model. Here we give a brief description of each of the three study sites, the tools used, and explain the experimental design.

2.1. Study Sites

The Kerguelen Plateau and Heard Island (southeast of the Kerguelen Island), depicted by the box on the right of Figure 1d (bathymetry plot), is a major bathymetry feature within the Indian Ocean sector of the Southern Ocean, extending from 46°S to 64°S at the 3000 m isobath. It forms a major barrier to the eastward flowing Antarctic Circumpolar Current (ACC), with most of the flow being deflected to the north of the plateau (∼100 Sv), and the substantial remainder to the south (30–40 Sv), steered primarily by the
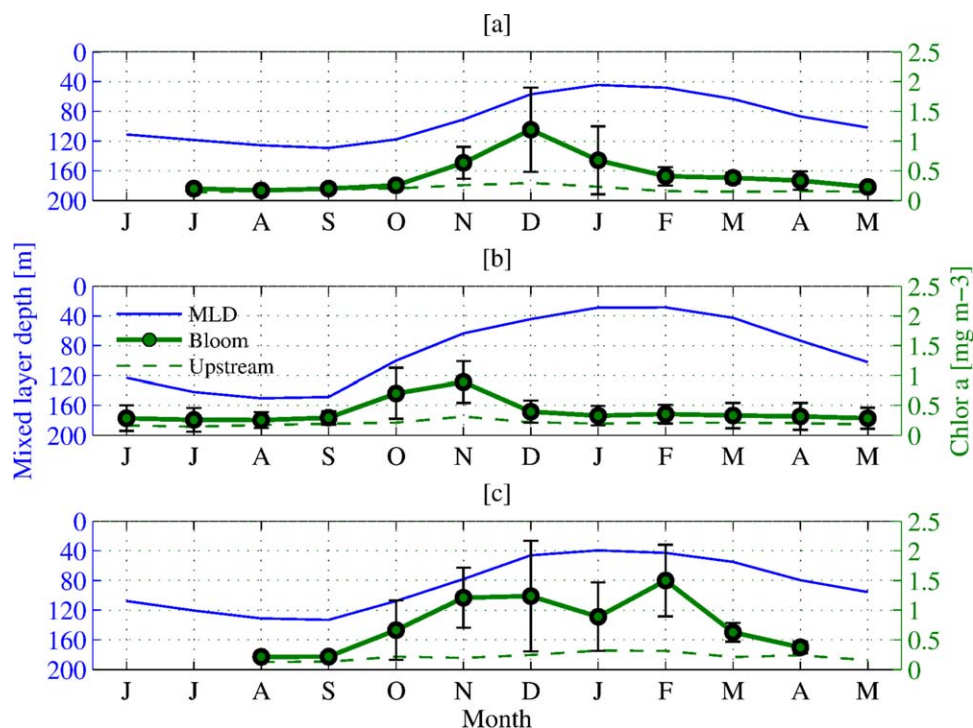
Figure 3. The average chlorophyll *a* concentration (mg m^{-3}) (satellite ocean color) of each month over the 10 year period. Concentrations are from two locations, one inside (thick green line with markers) and one outside of the bloom region (dashed green line), for each island. The data points from inside the bloom region include error bars which are plus and minus one standard deviation in chlorophyll *a* for each month, over the 10 year period. The blue line represents the decadal average of the mixed layer depth of each location inside the bloom. (a) Kerguelen, (b) Crozet, and (c) South Georgia. Note the *x* axis, "Month," begins from June to May.

topography. The circulation over the plateau between the two islands is rather stagnant, <5 cm^{-s} on average. A major circulation feature within the region is the Polar Front (PF), which cuts between the two islands, flowing close to the southeast Kerguelen Island [*Park et al.*, 2008a, 2008b, 2014]. The Kerguelen bloom occurs on decadal average during November to January, as demonstrated in Figure 3a, and is predominately made up of diatom species above the plateau [*Blain et al.*, 2001]. However, note that the Kerguelen bloom can persist for much longer periods, due to a concurrent resupply of essential nutrients via remineralization and entrainment from the deep ocean during vertical mixing [*Boyd*, 2007].

Crozet Islands (46°S, 52°E), depicted by the central black box in Figure 1d, are separated from the Del Cano Rise plateau to the west by the Subantarctic Front (SAF), which is the dominant circulation feature in the area. The SAF predominately lies west to east within the ACC, but turns sharply north between the two plateaus (Crozet and Del Cano Rise), before turning eastward to the north of Crozet as it comes into contact with the Agulhas Return Current [*Bakker et al.*, 2007; *Pollard et al.*, 2007]. Over the plateau and to the north of the island (bounded by the SAF) is an area of Polar Frontal Zone characterized by weak circulation (15–20 Sv), within which iron can accumulate during the winter months that can subsequently fuel a bloom [*Planquette et al.*, 2007]. The phytoplankton community structure of the Crozet bloom, described by *Poulton et al.* [2007], is made up of varying sizes of diatoms, and very small prymnesiophyte *Phaeocystis antarctica*. Biomass varies considerably near to the plateau between species, but further away from the plateau, to the northwest and east, prymnesiophyte *P. antarctica* can dominate.

South Georgia and Shag Rocks (northwest of South Georgia), hereafter referred to collectively as South Georgia, are located to the east of Drake Passage, highlighted by the left black box in Figure 1d. The islands form part of the North Scotia Ridge at roughly 54°S, 37°W, directly in the path of the ACC. The PF lies north of the islands, and the Southern ACC Front flows to the south, looping anticyclonically around South Georgia before flowing east again [*Orsi et al.*, 1995; *Meredith et al.*, 2003]. North of the island, enclosed by the PF and Southern ACC Front, is the South Georgia Basin, within which prolonged blooms exist throughout the

growing season [*Borrione and Schlitzer*, 2013]. This paper will focus on the South Georgia Basin bloom, but there are blooms occurring to the south and west of the islands [*Ward et al.*, 2007], although these blooms are partly subsurface and may not be represented by satellite observations. Furthermore, the region is one of the most productive regions across the entire Southern Ocean, with various sources of iron and phytoplankton [*Ardelan et al.*, 2010; *Murphy et al.*, 2013; *Thomalla et al.*, 2011]. Consequently, from satellite ocean color data alone, it is not possible to delineate blooms fertilized by iron from South Georgia sediments or from elsewhere within the basin (Antarctic peninsula or ice melt). The South Georgia Basin bloom (hereafter referred to as the South Georgia bloom) is dominated by large diatom species, but is described as "patchy" over scales of 10–20 km, with fragmented diatom colonies occurring alongside a more invariant community of small autotrophs and heterotrophs [*Atkinson et al.*, 2001; *Korb et al.*, 2008].

Each of the three islands has different characteristics which determine the ecosystem that they support and its functioning, but for a generalized overview of the Southern Ocean ecosystem, see *Boyd* [2002]. These islands have been selected for this study as their blooms have been extensively explored in the field [*Blain et al.*, 2008; *Pollard et al.*, 2007; *Korb et al.*, 2008; *Murphy et al.*, 2013], the results from which can be used to support our own analysis.

2.2. Satellite Data
2.2.1. Chlorophyll Observations
The ocean color data used in this study come from the ESA Ocean Colour Climate Change Initiative. Here we use a (level 3 geographically mapped) merged and bias corrected product from the MERIS, MODIS, and SeaWiFS data sets, with a horizontal resolution of up to 4 km [*Storm et al.*, 2013]. Because of the low solar elevation and sea-ice coverage in winter, data are unavailable in some areas, most visibly the Weddell Sea in Figure 1a, but by averaging over a month, year, and decade, we can fill in many of the gaps. This study has utilized monthly chlorophyll *a* (chl *a*) concentrations over the period 1998–2007, the first decade in which we have good satellite coverage across the world. In this study, the chlorophyll data are used to represent phytoplankton biomass, defining the island blooms.
2.2.2. Altimetric Sea Surface Currents
The satellite altimeter data are produced by Ssalto/Duacs and distributed by the Archiving Validation and Interpretation of Satellite Data in Oceanography (Aviso) group, with support from CNES (http://www.aviso.altimetry.fr/duacs/). Here we utilize a merged data set, from only two satellites at any one time, each having the same ground track and stable sampling which provides a homogenous time series. This along-track, delayed time data product has great stability and therefore is the ideal product for use in inter-annual comparison studies [*Le Bars et al.*, 2014].

The along-track Absolute Dynamic Topography (ADT) is obtained by adding the Sea Level Anomaly to the Mean Dynamic Topography (Mean Sea Surface Height minus Geoid). A mapping procedure using optimal interpolation with realistic correlation functions is applied to produce ADT maps (MADT or L4 products) onto a Cartesian $1/4° \times 1/4°$ grid [*Aviso*, 2014]. Here we use the sea surface geostrophic velocities computed from the ADT over the period of 1998–2007.

2.3. NEMO Model and Ariane Lagrangian Particle Tracking
The NEMO 1/12° resolution ocean general circulation model has been developed with particular emphasis on realistic representation of fine-scale circulation patterns [*Madec*, 2008], which provides an ideal platform to conduct Lagrangian particle-tracking experiments around the small islands of the Southern Ocean. Full details of the model run, including model setup and configuration, can be found in *Marzocchi et al.* [2015] as only a brief description will be given here. The model is initialized with World Ocean Atlas (WOA) 2005 climatological fields and forced with 6 hourly winds, daily heat fluxes, and monthly precipitation fields [*Brodeau et al.*, 2010]. The run begins in 1978, with output through to 2010, of which we are interested in 1998–2007. Model output is stored offline as successive 5 day means throughout the model run, of which the velocity fields are used for the particle tracking in this paper.

The Ariane package [*Blanke and Raynaud*, 1997] (available online at: http://stockage.univ-brest.fr/~grima/Ariane) is applied to the NEMO velocity field to track water parcels using point particles that are released into the modeled ocean circulation (cf. *Popova et al.* [2013] and *Robinson et al.* [2014], who used output from the NEMO 1/4° model). These particles are intended here to represent water masses fertilized by iron

scoured from the island sediments. Further details about the Ariane package can be found in *Blanke and Raynaud* [1997] and *Blanke et al.* [1999].

An important caveat to the results is that we do not expect the NEMO 1/12° model to reproduce the detailed mesoscale flows year-by-year due to chaotic dynamics, as the mesoscale eddy field is not initialized to match that of the real world (only possible using data assimilation). Nevertheless, the model does reproduce the larger-scale flow field in the vicinity of the islands, which is important for downstream advection (see Figures 1b and 1c).

2.4. Experiment Design

In order to study the advection of iron from island sources and make a qualitative comparison with the ocean color 1998–2007 observations, Lagrangian particles were released monthly into the modeled circulation from around the shelf regions of each island, from January 1998 to December 2007. Particles are deployed in every other grid cell of the 1/12° model grid along the horizontal (latitudinally and longitudinally), and at each level of the NEMO grid depth domain down to a maximum depth of 180 m (30 depth levels, not equally spaced see *Madec* [2008]), around each of the three islands (cf. *Srokosz et al.* [2015], who used a similar analysis for the Madagascar bloom). Figure 2 shows the starting positions of the particles around each of the islands. The particles had to be spaced at a high enough resolution to resolve the fine-scale circulation patterns around each island, but the experiments were limited computationally, as the islands are not of a comparable area, so there could not be a particle within every model grid cell. The particles are released in both the horizontal and vertical extent, to represent iron that is scoured from the shelf sediment (down to 180 m in this experiment) and mixed upward [*Ardelan et al.*, 2010; *Blain et al.*, 2001; *Hewes et al.*, 2008; *Planquette et al.*, 2007] as well as other island sources, such as river runoff [*van der Merwe et al.*, 2015]. Particles that are subducted deeper than 200 m, i.e., out of the euphotic zone, along their trajectory are removed from the analysis. At the horizontal and vertical grid spacing described, that results in 8240 Lagrangian particles being released each month from the Kerguelen and Heard Island, 465 particles from Crozet, and 2820 particles from South Georgia and Shag Rocks.

2.4.1. Assumptions and Limitations of Method

The main assumption in this study is that surface waters in the Southern Ocean are iron limited, and that the addition of iron to an area, via horizontal advection, would initiate a bloom. However in reality, productivity can be colimited in the Southern Ocean, with light or silicate, for example, and there are also seasonal factors which control phytoplankton growth, which can vary in both time and space [*Boyd*, 2002].

In the analysis to follow, the advection time over a period of 12 months is discussed. Note that the residence time of bioavailable iron in surface waters is not yet fully understood, but thought to be relatively short, on the order of only weeks to months [*Boyd and Ellwood*, 2010; *Shaked and Lis*, 2012; *Schallenberg et al.*, 2016]. However, studies have also shown that iron can be transported during winter months and remain in the upper ocean to be available to stimulate blooms in the summer months [*Mongin et al.*, 2009; *d'Ovidio et al.*, 2015]. *Graham et al.* [2015] postulates that this might be possible due to intense biological recycling of iron, or the long-range transport of particulate iron, or even by currently unknown processes. For the time being, these questions remain unanswered, and so for the purpose of this study all of the iron from the islands is assumed to remain available throughout the year. A further assumption is that all advective pathways have the potential to be fertilized with iron.

A caveat to this analysis is that, in using satellite ocean color data, it is not possible to detect subsurface chlorophyll maxima, which are known to exist in certain regions of the Southern Ocean [*Holm-Hansen et al.*, 2005; *Tripathy et al.*, 2015]. Therefore, we cannot use our analysis to draw any conclusions on the location or variability of known subsurface chlorophyll maxima [*Ward et al.*, 2007], and make the distinction now that only surface blooms are considered, hereafter just referred to as blooms.

As touched upon in section 1, the representation of iron and its transport in this method is a simplification. Ideally, this study would be performed using tracers in a high-resolution, fully coupled biogeochemical model, but the computational resources required for this would be extreme. Such a study would need a coupled model at a resolution high enough to formally resolve the small-scale circulation features that occur around the islands at the center of this study. As such, the analysis presented in our results and discussion is restricted to consider only potential iron advection and consequent fertilization.

3. Results

3.1. Ocean Color

Figure 1a is a 10 year average of satellite-derived sea surface chl a concentrations in November, over 1998–2007. The islands of interest are highlighted by black boxes, from which it is clear that these island blooms can be more than double the magnitude of productivity anywhere else in the Southern Ocean. Figure 3 is the decadal monthly averages, of surface chl a concentration, for a single location inside, and a single location outside of the bloom sites for each island. Each location was selected arbitrarily based on persistence either inside or outside (upstream of the ACC) of the annual bloom. The latitude and longitude coordinates of each location inside the bloom are 72°E and 49°S, 52.5°E and 45.5°S, and 38.5°W and 52.5°S for Kerguelen, Crozet, and South Georgia, respectively. The coordinates of each location upstream of the bloom are 66°E and 48°S, 45.5°E and 46.5°S, and 49.5°W and 52.5°S (cf. *Park et al.* [2008a, 2008b, Figure 11], *Pollard et al.* [2009, Figure 1], and *Korb et al.* [2004, Figure 1], for schematic positioning of the ACC around Kerguelen, Crozet and South Georgia respectively). In this paper, a bloom is defined by chl a concentrations higher than 0.5 mg m^{-3}, as it is consistently higher than chl a outside of each islands typical bloom regions [*Comiso et al.*, 1993; *Moore and Abbott*, 2000]. Also, when 0.5 mg m^{-3} of chl a is exceeded in Figure 3, it occurs on a steep gradient from 1 month to the next, indicating the start of a bloom. Additionally, this concentration is low enough to avoid complications with double peaks in chl a associated with South Georgia, as can be seen in Figure 3c. South Georgia is a region that frequently has two bloom peaks per year [*Borrione and Schlitzer*, 2013]; however, it is outside of the scope of this work to analyze peak bloom events. Therefore, in order to focus on inter-annual rather than inter-seasonal variability, we consider the average chl a concentration over the bloom period. The error bars in Figure 3 are 1 standard deviation in chl a for each month, over the 10 year period. The size of the error bars is an indication of the seasonality across the regions and annual cycles. South Georgia, in particular, has large error bars which are due to the range in magnitude of annual blooms. For instance, the average chl a for January over 1998–2007 is <1 mg m^{-3}, however, in January of 2002, the concentration was as high as 15 mg m^{-3} [*Korb and Whitehouse*, 2004].

Figure 3 also includes the averaged (decadal) monthly mixed layer depth (MLD) in the "bloom" site for each island, calculated online in the NEMO model. Comparing the bloom and MLD curves, we see that the bloom is likely triggered by the onset of a shallowing mixed layer [*Venables and Moore*, 2010]. The MLD, specifically its role in terminating the blooms, is considered in further detail in the discussion.

Figure 4 shows example years of a small and a large averaged bloom period (hereafter referred to as the bloom) for each island, during 1998–2007. Maximum and minimum blooms for Kerguelen occur in 2003 and 2000, Crozet is 2004 and 2001, and South Georgia is 2002 and 2006. Strikingly, Figure 4 demonstrates the strong inter-annual variability in both bloom magnitude and area, which may be explainable by studying the potential iron advection from the islands.

3.2. NEMO Versus Aviso Surface Current Speed

The ability of the chosen model to accurately represent the circulation in the study area is critical to the quality of the results. In order to assess the performance of the NEMO 1/12° model, we can compare with satellite-derived sea surface currents (Aviso). The Aviso data are the geostrophic component of the velocity, whereas the NEMO model is the absolute velocity, but this should not impact a comparison between the two as they are near equal at the surface. By comparing the decadal averages of NEMO and Aviso, side by side (Figure 1), we can assess the models performance.

Figures 1b and 1c are a comparison of the decadal (1998–2007) average ocean surface current speed, from NEMO and Aviso, respectively, across the Southern Ocean. Qualitatively, the model correctly captures the major features, and also their magnitude. Fast flowing currents are stronger in the model than Aviso, and also boundaries of fast flowing currents within the modeled circulation are more defined than in the observations. This may be due to data smoothing caused by the correlation function applied to the Aviso data or due to the model under representing submesoscale features. Figures S1–S3 in the supporting information show the decadal, annual, and monthly averaged circulation, of both model and satellite-derived velocities, for each island for illustrative purposes.
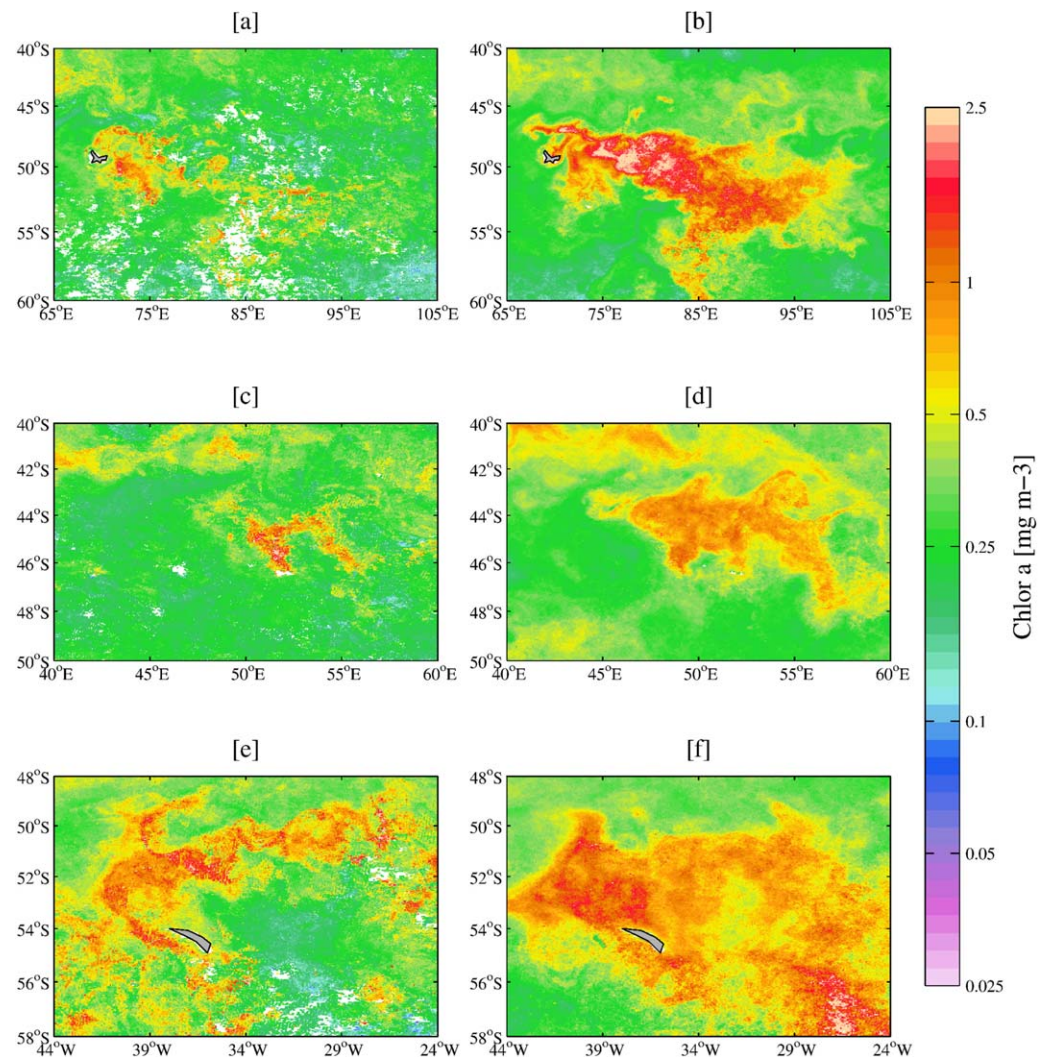
Figure 4. Example years of satellite ocean color plots of each island. Chlorophyll *a* concentrations have been averaged over the bloom period for each year. The top row is Kerguelen (bloom period: November–January), years (a) 2000 and (b) 2003; the middle row is Crozet (bloom period: October–December), years (c) 2001 and (d) 2004; and the bottom row is South Georgia (bloom period: October–April), years (e) 2006 and (f) 2002. Figures 4a, 4c, and 4e are examples of a small bloom extent during the 1998–2007 year period, and Figures 4b, 4d, and 4f are years with a large bloom extent.

3.3. Advection of Iron Toward the Bloom Site

In this paper, we hypothesize that the advection of iron downstream of islands allows blooms to occur in the otherwise high-nutrient, low-chlorophyll regime of the Southern Ocean. Here we investigate the time scales of fertilization, and the degree to which the circulation can impact inter-annual variability, during the period 1998–2007.

The Kerguelen bloom occurs on decadal average during November to January, as demonstrated in Figure 3a. For this analysis, we focus on the average surface chl *a* concentration over the bloom period (November to January in Kerguelen's case) for each year, referred to as the bloom. Figure 5 shows the patch around Kerguelen that could potentially be fertilized with iron by the local circulation in the NEMO model. The fertilized patch is depicted by colored markers, which represent the location of trajectories in October for each year, with the different colors indicating the month in which the particles were released from the island. Strikingly, the fertilized patch is much larger than the bloom extent, represented by black contours in each annual subplot. The trajectories propagate east from the island between the latitude band of roughly 45°S–54°S, but then spread both northward and southward in extent from roughly 77°E. However, despite the fertilized patch reaching as far north as 40°S in Figure 5, we can see from the black contours that the bloom area is never north of 45°S in any of the years.
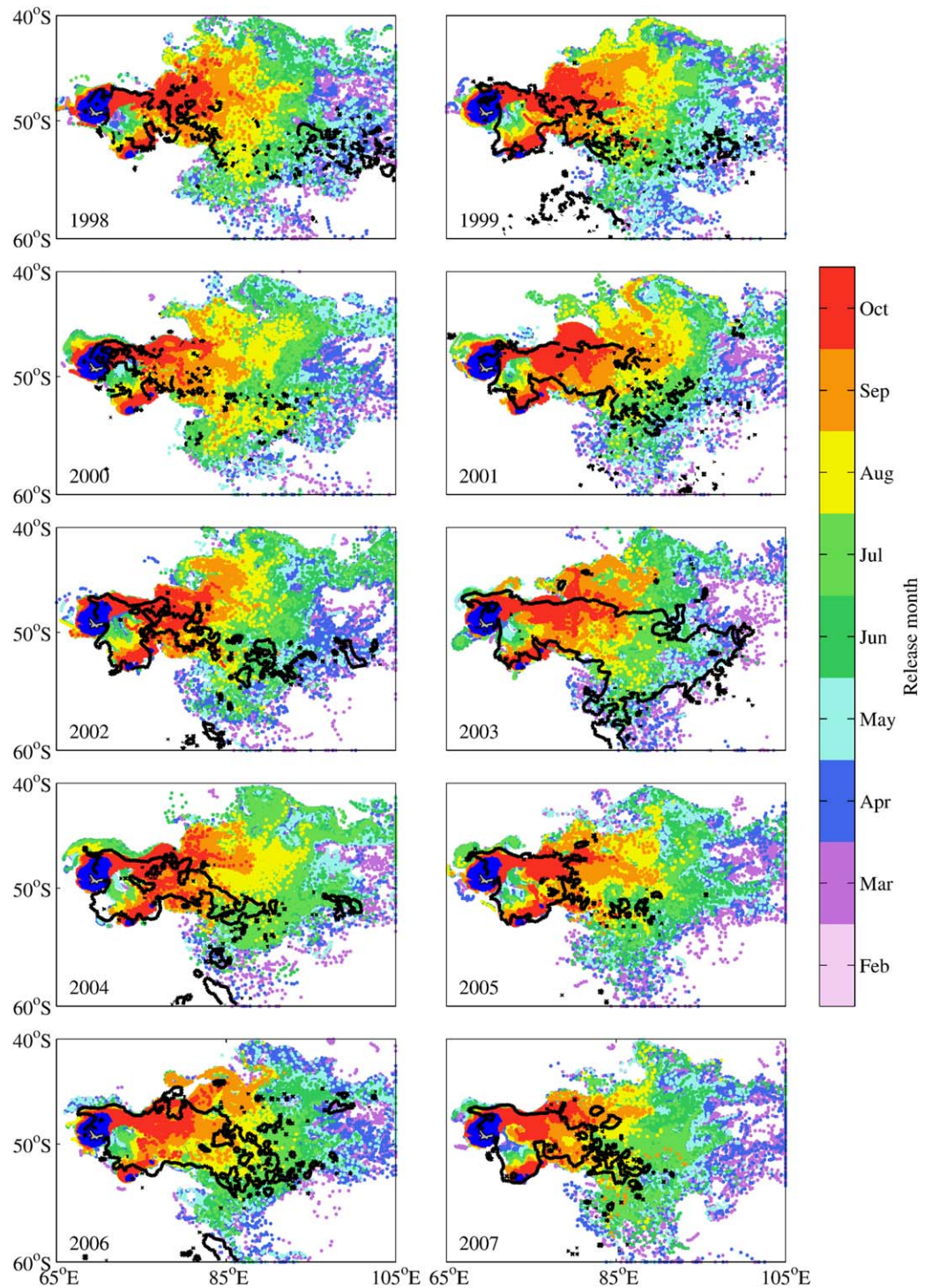
Figure 5. Extent of Lagrangian trajectories around Kerguelen. Eight thousand two hundred forty particles were released monthly from their starting positions, denoted in blue; however, only every second particle is shown here for clarity. Particle trajectories in October (preceding the start of the bloom) are depicted by colored markers. The color of the trajectory relates to the month in which it was released as indicated by the color bar. The black contour represents the averaged bloom area, over November–January, of chlorophyll *a* concentrations above 0.5 mg m^{-3}. Only trajectories that are shallower than 200 m are included in this plot.

Having found that the horizontal advection of iron would be sufficient to fertilize the bloom in principle, a further question arises as to whether the bloom is terminated by the exhaustion of iron in the surface water. This question cannot be addressed directly using the NEMO 1/12° simulation, as it is not a coupled
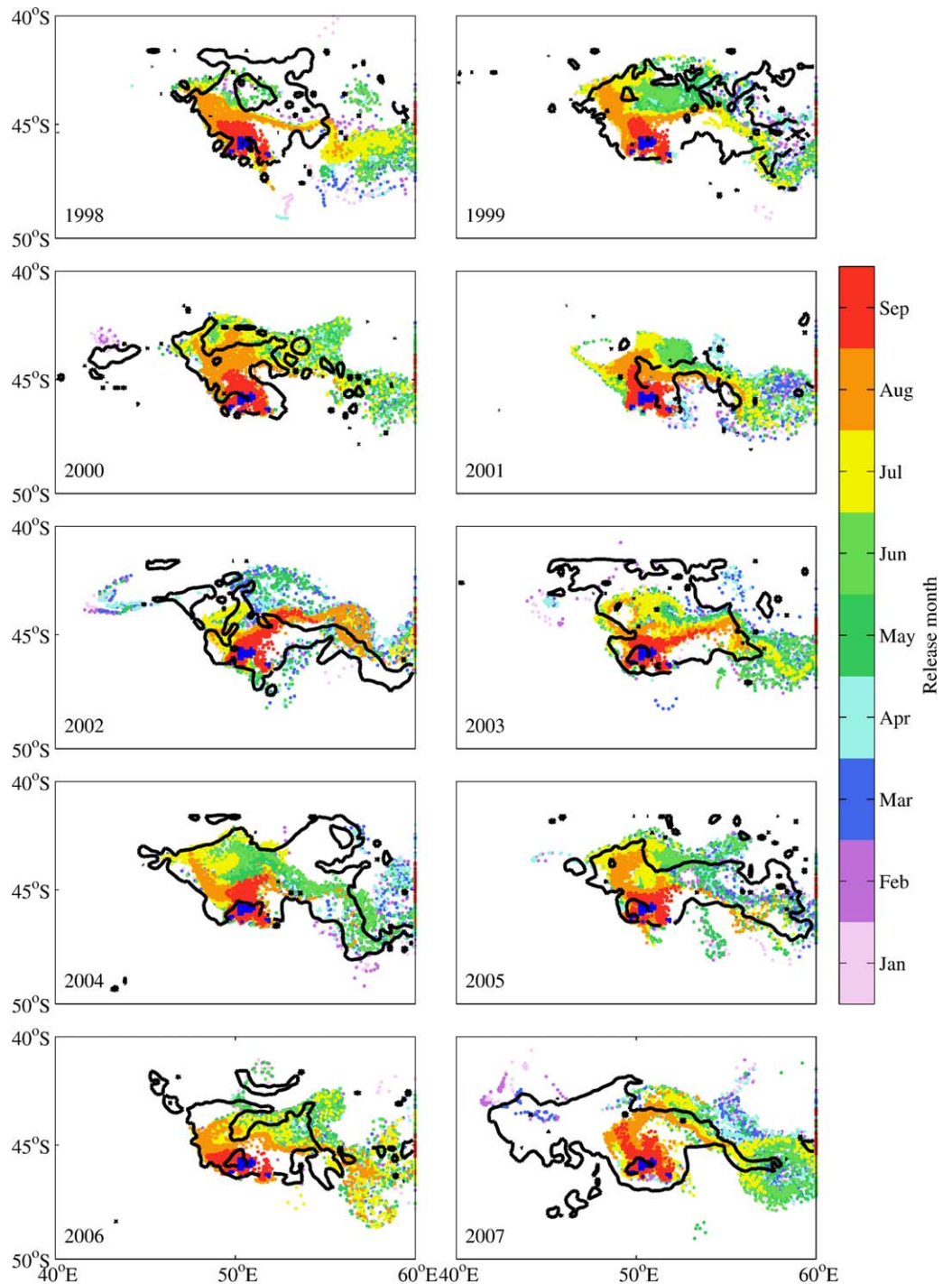
Figure 6. Extent of Lagrangian trajectories around Crozet. Four hundred sixty-five particles were released monthly from their sing positions, denoted in blue; however, only every second particle is shown here for clarity. Trajectories in September (preceding the start of the bloom) are depicted by colored markers. The color of the trajectory relates to the month in which it was released as indicated by the color bar. The black contour represents the averaged bloom area, over October–December, of chlorophyll a concentrations above 0.5 mg m^{-3}. Only trajectories that are shallower than 200 m are included in this plot.

biogeochemistry model. However, if the bloom is terminated by the exhaustion of iron then a question that can be addressed is: can advection resupply iron in the period between the end of one bloom and the start of the next? as addressed by *Mongin et al.* [2009], and more recently by *d'Ovidio et al.* [2015]. For Kerguelen, the location of the fertilized patch was very consistent, however, there are temporal differences in the
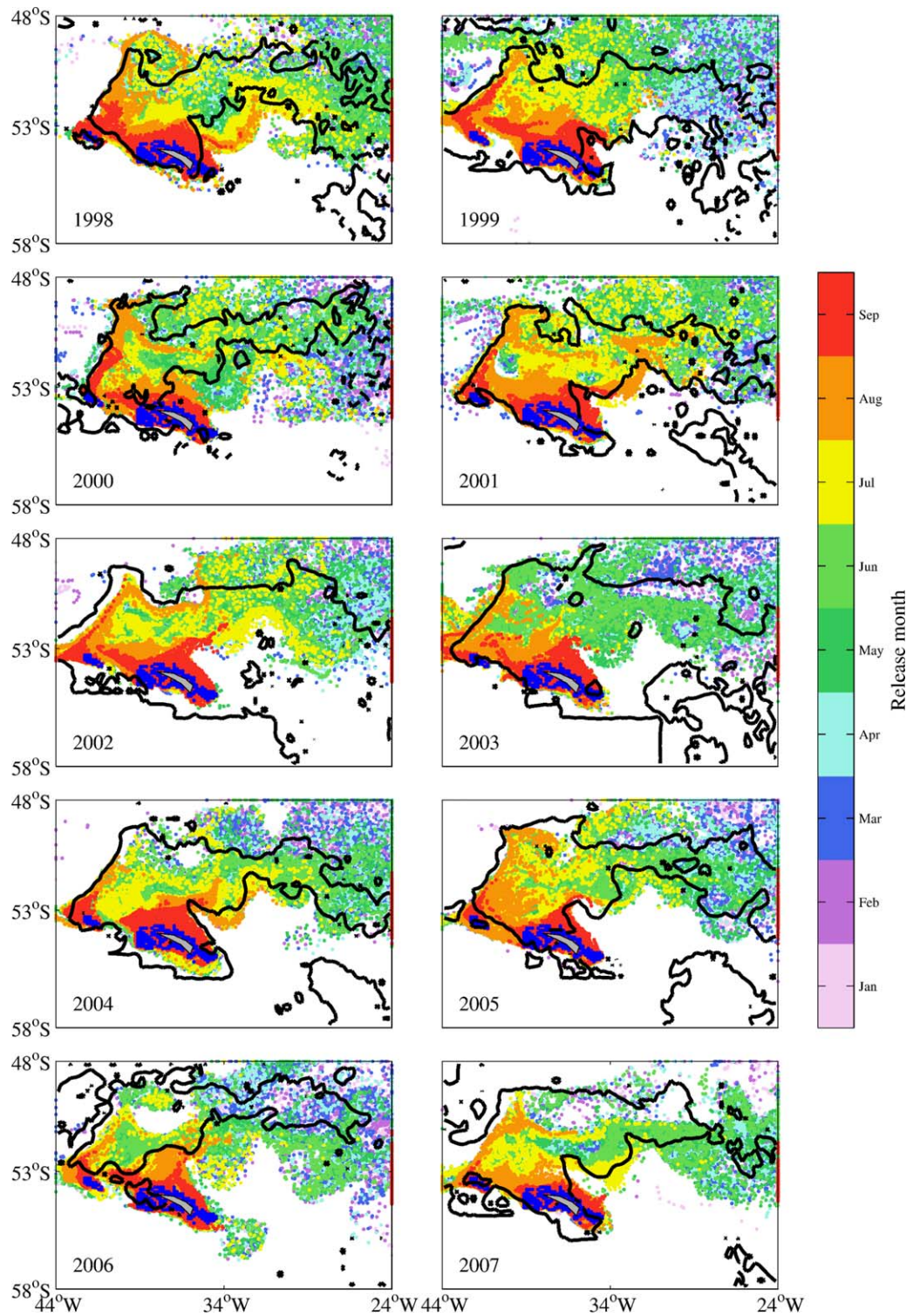
Figure 7. Extent of Lagrangian trajectories around South Georgia. Two thousand eight hundred twenty particles were released monthly from their starting positions, denoted in blue; however, only every second particle is shown here for clarity. Trajectories, in October (preceding the start of the bloom), are depicted by colored markers. The color of the trajectory relates to the month in which it was released as indicated by the colorbar. The black contour represents the averaged bloom area, over October–April, of chlorophyll a concentrations above 0.5 mg m^{-3}. Only trajectories that are shallower than 200 m are included in this plot.

Table 1. Size of the Annual Bloom and Fertilized Patch Around Kerguelen, and the Percent of Each Area That Is Overlapped by the Other[a]

Year	Bloom Area (km^2)	Fertilized Patch (km^2)	Bloom Overlap (%)	Fertilized Overlap (%)
1998	674,572	2,731,476	74	18
1999	803,847	2,676,533	64	19
2000	339,783	2,693,883	78	10
2001	832,765	2,593,000	84	27
2002	613,450	2,621,786	75	18
2003	1,602,173	2,435,464	73	48
2004	729,515	2,637,034	72	20
2005	532,218	2,568,354	84	17
2006	1,056,154	2,539,699	82	34
2007	640,068	2,358,635	86	23

[a]Bloom Area is the total area of the average (November–January) chl a concentration above 0.5 mg m^{-3}; Fertilized Patch is the extent of particle trajectories in October (prior to the start of the bloom); Bloom Overlap is the percent of the bloom area overlapped by the fertilized patch; Fertilized Overlap is the percent of the fertilized patch overlapped by the bloom.

timing of advection. Nevertheless, the results show the maximum advection time for the particles to reach the furthest extents of the bloom is on the order of 5–6 months, suggesting that horizontal advection is sufficient to resupply the bloom area with iron, in agreement with *Mongin et al.* [2009] and *d'Ovidio et al.* [2015].

Figure 6 is the same as 5, but focusing on Crozet. The Crozet bloom occurs 1 month earlier than the Kerguelen bloom, on decadal average during October to December [*Pollard et al.*, 2007], and so the trajectories shown in Figure 6 represent the fertilized patch in September. Figure 6 suggests that there is more inter-annual variability in the circulation around Crozet than Kerguelen, both spatially and temporally. In Figure 6, the fertilized patch tends to be north of the island and to the east, made up of particles released in June–August (light green to orange on the color bar). This indicates that the time scale for fertilization, of water mass being within the immediate vicinity of Crozet (where the particles are released) to outside of the bloom area (the black contours), is on the order of 3–4 months; however, Figure 6 clearly shows the inter-annual variability in this time scale. There are some years in Figure 6 where we see the fertilized patch extending to the west of the island, most visibly in the years 2000, 2002, 2003, and 2007. The color of the markers seen to the west of the island in some of the years show the particles were released earlier in the year, ranging from January (2000) to April (2002). Focusing on the black contours in Figure 6, representing chl a concentrations above 0.5 mg m^{-3} during the bloom period, there are years in which the bloom is propagated to the west also, most clearly apparent in 2000 and 2007.

The bloom associated with South Georgia occurs on decadal average, during October to April; however, South Georgia experiences the highest seasonality of all the three islands in this study. Here we discuss the South Georgia bloom, although the surrounding area is one of the most productive regions within the Southern Ocean [*Ardelan et al.*, 2010; *Young et al.*, 2014], so separating a bloom associated with iron-only advected from South Georgia is not nontrivial. In order to address this issue, we have applied a mask to the ocean color data, to remove chl a that was most likely fertilized from other iron sources in the region, guided by the surface chl a climatology around South Georgia produced by *Borrione and Schlitzer* [2013]. Figure 7 is again the same as Figures 5 and 6, with the colored markers representing the particle locations in September (preceding the start of the bloom). The extent of the fertilized patch around South Georgia changes annually, although to a lesser degree than around Crozet. What does remain almost annually consistent is the north and eastward advection of the particles (with the exception of 2006) and an associated bloom occurring within the Georgia Basin, which is just north of the island. In some of the years, most distinctly in 2004 and 2005, there is a well-defined boundary edge to the trajectories on the western side of the fertilized patch. This sloping western boundary edge is also apparent in the average bloom area in almost all years (2006 being the most apparent exception). The trajectories and bloom are restricted to the east of this boundary due to the eastward flowing PF which acts as a physical barrier [*Moore et al.*, 1999; *Korb and Whitehouse*, 2004]. The colored markers represent the particles locations in the month of September, and therefore particles that are released at the beginning of September have only had 1 month to be advected, and consequently are the closest to South Georgia. Focusing just on the recently released particles, from August and September (orange and red), it is apparent that, for the majority of the years, this western boundary of both the fertilized patch and bloom area is an important route for iron to be advected away from South Georgia, flowing toward Shag Rocks and then along the PF. This circulation feature was also found by *Young et al.* [2011] in their higher-resolution regional model, described as a unidirectional link between the two land masses (see their Figure 7).

Table 2. Size of the Annual Bloom and Fertilized Patch Around Crozet, and the Percent of Each Area That Is Overlapped by the Other[a]

Year	Bloom Area (km^2)	Fertilized Patch (km^2)	Bloom Overlap (%)	Fertilized Overlap (%)
1998	223,784	216,357	35	36
1999	300,810	251,913	52	62
2000	168,707	259,734	59	38
2001	70,586	231,342	60	18
2002	195,589	238,834	42	34
2003	299,167	232,525	41	52
2004	355,097	252,176	48	67
2005	258,354	246,721	54	56
2006	209,982	244,683	47	40
2007	342,084	282,999	32	39

[a]Bloom Area is the total area of the average (October–December) chl a concentration above 0.5 mg m^{-3}; Fertilized Patch is the extent of particle trajectories in September (prior to the start of the bloom); Bloom Overlap is the percent of the bloom area overlapped by the fertilized patch; Fertilized Overlap is the percent of the fertilized patch overlapped by the bloom.

Table 1 provides the size of both the annual blooms and fertilized patches around Kerguelen. As can also be seen in Figure 5, the fertilized patch is much larger than the bloom, and there is more variability in the bloom size than in the fertilized patch. Consequently, the annual percentage of the bloom area that is within the fertilized patch is consistently very high, with an average of 77% (st dev ±6.5). As the fertilized patch is much larger than the bloom area, it would suggest that iron availability is not the only, or at least most important, factor controlling the Kerguelen bloom extent and inter-annual variability. The year 2003 had the largest bloom in our study period, in which the bloom did extend out across and to the southern edges of the fertilized patch. It is possible, that in 2003 the primary limiting factor to the Kerguelen bloom was alleviated so the bloom could extend further out into the regions of available iron. This hypothesis will be considered later in the study.

Looking at Table 2, the Crozet bloom is a third of the size of the Kerguelen bloom, with an average bloom size of 242,416 km^2 compared to the Kerguelen average of 782,455 km^2. Focusing on the percentage of the bloom site overlapped by the trajectories (*Fertilized patch*) for each year, there is a range of 60%–32% overlap. This is reflected in the percentage of the fertilized patch overlapped by the bloom, ranging from 67% to 34%. Both the bloom area and fertilized patch around Crozet vary annually, and Crozet has the lowest overlap out of the three islands studied.

The average size of the South Georgia bloom over 1998–2007 was 618,645 km^2, smaller than the average size of the fertilized patch at 742,038 km^2. In Table 3, we can see a large range in the bloom area around South Georgia across the years, the maximum being 946,833 km^2 in 2002 and the minimum being 414,108 km^2 in 2006 (see Figure 4). There is also a range in the size of the fertilized patch, although not as large as the range in bloom size. Focusing on the amount of overlap between the bloom and trajectories, we see that the annual bloom overlaps are generally larger than the fertilized patch overlaps (2002 and 2003 being the exceptions). This is due to the fertilized patch being larger than the bloom area for the majority of the years. However, as with the other two islands, there is a range in the annual overlaps, which can be explained by a combination of inter-annual variability in the sizes and locations of the annual blooms, and also, to differing degrees for each island, the inter-annual variability in the size and locations of the fertilized patches (Kerguelen being the most consistent, and Crozet exhibiting the most variation).

Table 3. Size of the Annual Bloom and Fertilized Patch Around South Georgia, and the Percent of Each Area That Is Overlapped by the Other[a]

Year	Bloom Area (km^2)	Fertilized Patch (km^2)	Bloom Overlap (%)	Fertilized Overlap (%)
1998	527,788	801,679	79	52
1999	671,337	864,382	70	54
2000	453,359	810,443	79	44
2001	560,929	798,532	74	52
2002	946,833	704,231	50	67
2003	854,692	750,085	56	64
2004	587,281	713,427	69	57
2005	626,285	700,466	66	59
2006	414,108	703,676	56	33
2007	543,833	573,456	61	58

[a]Bloom Area is the total area of the average (October–April) chl a concentration above 0.5 mg m^{-3}; Fertilized Patch is the extent of particle trajectories in September (prior to the start of the bloom); Bloom Overlap is the percent of the bloom area overlapped by the fertilized patch; Fertilized Overlap is the percent of the fertilized patch overlapped by the bloom.

Figure 8 shows the overlap of the bloom (bloom period average, chl a concentration greater than 0.5 mg m^{-3}) by the fertilized patch from each individual monthly release of particles. In the Kerguelen plot, we see a maximum range of around 10–25% between years, in the overlap between monthly releases of particles and the average bloom. The cause of this range is a combination of inter-annual variability in both the advection and bloom extent. In comparison with Figure 5 and Table 1, it is apparent that the highest degree of variability
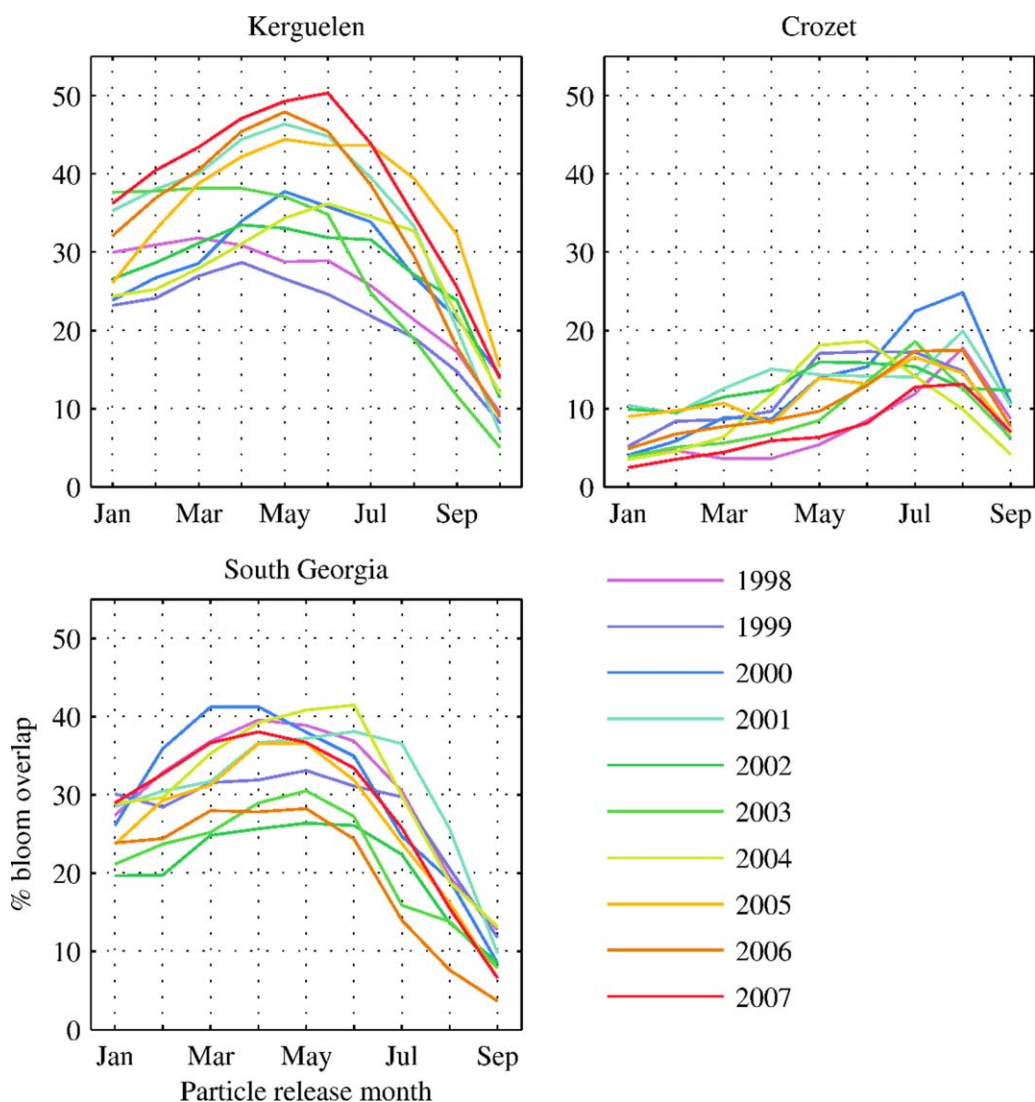
Figure 8. The percent of the bloom area overlapped by Lagrangian trajectories from each monthly release for each year. For each monthly release of particles, trajectories that were within the bloom area, in the month that is prior to the start of the bloom, were recorded and used to calculate the percentage area coverage of the bloom by Lagrangian trajectories. Any particles deeper than 200 m were not included. The y axis, *% bloom overlap*, indicates the percentage of the bloom area overlapped by particles from each monthly release shown on the x axis, *Particle release month*. Each colored line represents an individual year.

comes from the bloom, although the inter-seasonal variation in advection timing and consequently fertilization could also impact bloom development. Particles released in October, just prior to the start of the bloom, cover around 10–15% of the bloom area, with the maximum bloom coverage from releases in April–June for the majority of the years. This gives an advective fertilization time scale of between 5 and 7 months for maximum bloom coverage. The circulation on the Kerguelen Plateau itself is known to be sluggish, certain parts even described as stagnant [*Park et al.*, 2014]. This localized slow moving water on the plateau (where particles start) may account for the low bloom overlap percentage by particles released just prior to the start of the bloom (November).

In Figure 8, Crozet shows less inter-annual variability than Kerguelen, of less than 10% difference between years. The most apparent difference between Crozet, and the other two islands, is that the advective fertilization time scale is much shorter, with maximum bloom overlap from particles released in June–August, which is 2–4 months prior to the start of the bloom (typically October). However, Crozet has the lowest bloom overlap, with a maximum of 25% from an August release in 2000. For the majority of the years, the maximum percent coverage of the bloom is below 20%.
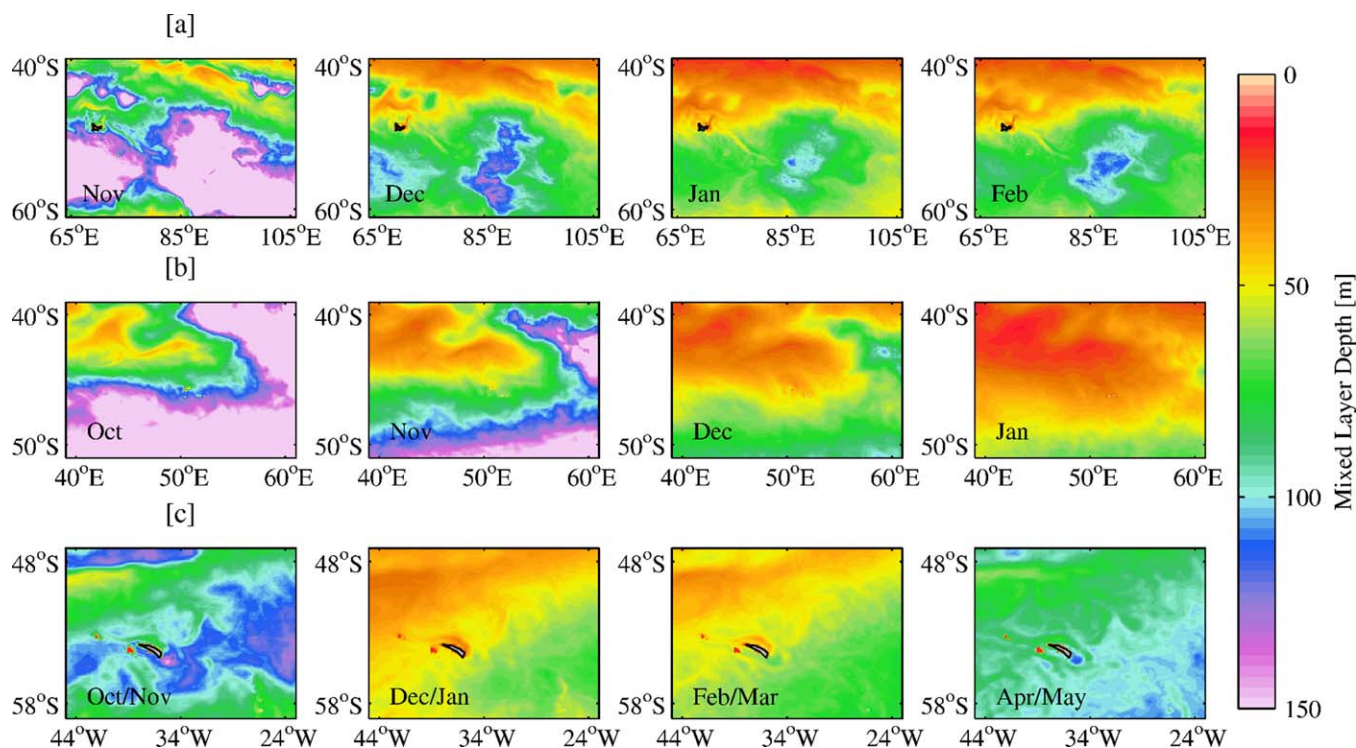
Figure 9. Monthly climatologies (decadal, 1998–2007) of the modeled mixed layer depth, calculated online by the NEMO model, around Kerguelen, Crozet, and South Georgia. The color scale is meter below the surface, with warm colors indicating shallow depths and cold colors representing deeper depths.

The South Georgia plot of Figure 8 shows a degree of consistency in the timing of fertilization, but high variability in the bloom overlap from each monthly release, across the years. The variability in bloom overlap is on the order of 10–15%, and the advective fertilization time scale is roughly April–June, 4–6 months prior to the typical start of the bloom. The maximum percentage bloom overlap is 40%.

4. Discussion

Here we consider other factors that could impact the bloom, light limitation, and nutrient control, before addressing our three main research questions: Can advection explain the extent of the bloom area? Can advection explain the bloom inter-annual variability? And what factors could cause bloom termination?

4.1. Light Limitation

In addition to iron limitation in the Southern Ocean, light limitation also plays an important role in controlling productivity [*Wadley et al.*, 2014]. The light levels encountered by phytoplankton cells is partly determined by the mixed layer depth (MLD), as they are vertically mixed between high surface irradiance and low subsurface irradiance (*Venables and Moore* [2010]—explanations and references therein). To assess the light availability around the islands during the typical bloom periods, Figure 9 shows the decadal average monthly depths of the mixed layer, calculated online in the NEMO model, over 1998–2007.

The top row of Figure 9 shows the MLD around Kerguelen which remains in a similar spatial pattern during the bloom period, with a distinct divide between the shallower north and deeper south. During the period 1998–2007, the Kerguelen bloom is constrained to the south of this divide where the MLD is deepest. The middle row shows the MLD around Crozet which exhibits the typical shallowing north to south of the MLD from winter into summer. In Figure 9, the bottom row is a 2 month decadal average of the mixed layer for the South Georgia region. Two months have been averaged together in order to capture the entire bloom period within the plot, from which we can see the typical north to south shallowing of the mixed layer from winter into summer. Both the Kerguelen and Crozet Islands blooms have typically terminated when the mixed layer is shallow enough for there still to be light available, which suggests that neither bloom is terminated by light limitation [*Venables et al.*, 2007; *Venables and Moore*, 2010]. The South Georgia bloom,
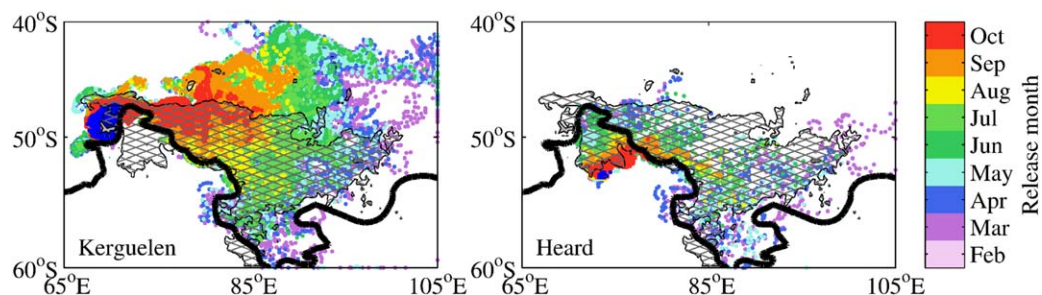
Figure 10. Lagrangian trajectories originating from the Kerguelen and Heard Islands in 2003. Collectively, 8240 particles were released monthly from their starting positions, denoted in blue; however, only every second particle is shown here for clarity. Particle trajectories are depicted by colored markers, with the color of the marker relating to the month in which it was released as indicated by the color bar. Gray hatching represents the bloom area, averaged over November–January, where chlorophyll a concentrations are above 0.5 mg m^{-3}. The thick black contour represents the approximate location of the Polar Front in the model for 2003. Only trajectories that are shallower than 200 m are included in this plot.

however, persists for the entire season and typically ends when the mixed layer begins to deepen in winter, strongly indicating that the bloom is terminated by diminishing light, and not by the exhaustion of iron.

4.2. Nutrient Control

The depth of the mixed layer is also significant for the amount of nutrients being brought to the surface from the deep, such as nitrate and silicate as well as iron. WOA climatologies show the concentration of nitrate to be high across much of the Southern Ocean, south of the Subantarctic Front, whereas silicate concentrations decrease rapidly north of the Polar Front [*Boyer et al.*, 2013]. At Kerguelen, during the recent KEOPS 2 cruise (October–November 2011), *Lasbleiz et al.* [2014] found higher concentrations of silicate south of the PF at roughly 72°E, close to the plateau.

One possible hypothesis is that silicate is the primary limiting factor controlling the large and highly variable Kerguelen offshore bloom (i.e., longitudinally far away from the plateau), both in spatial extent and interannual variability. This could explain why the bloom is contained to the south (bloom northern limit of 44°S), where a deeper MLD can mix silicate to the surface, despite the iron potentially being advected and available as far north as 40°S (see Figure 5). Many previous Southern Ocean iron fertilization studies, both artificial and natural, have reported the development of a large diatom bloom in the fertilized patch [*Blain et al.*, 2001; *de Baar et al.*, 2008; *Mongin et al.*, 2008] and consequently, in the region of Kerguelen, depletion of silicate over the plateau [*Mosseri et al.*, 2008]. The absence of a nondiatom bloom is explained by the efficient grazing of microbial communities by copepods and salps as suggested by *Banse* [1996] and *Smetacek et al.* [2004]. However, the majority of studies have been focused on the bloom above the plateau rather than further downstream, whereas the 2011 KEOPS II cruise focused mainly on the bloom located just northeast of the Kerguelen Islands above the abyssal plain. Their results suggest that the majority of diatom silica production during the bloom event is sustained by "new" silica, supplied primarily from prebloom winter water and also vertical supply. As the bloom progresses, the silicon pump is strengthened by the sinking of biogenic silica, and consequently the standing stock of available silica diminishes over time. Estimates for the duration of the high-productivity bloom period are on the order of 85–86 days, after which the bloom declines [*Mongin et al.*, 2008; *Closset et al.*, 2014]. These conditions could also be true of the far offshore bloom, which in some years extends further east than 95°S (2003, in Figure 5), but further in situ observations, of both silicate concentrations and bloom composition, would be necessary to either prove or disprove this.

4.3. Can Advection Explain the Extent of the Bloom Area?

Focusing now on the circulation around each island, we discuss if the modeled advection can explain the spatial extent of the island blooms. Our results suggest that iron advected from the Kerguelen and Heard Islands could fertilize an area which overlaps the annual bloom extent, but is actually much larger than the area of the bloom. Figure 10 shows that the bloom which occurs over the plateau (southeast of the Kerguelen Island) is predominantly fertilized by iron advected from Heard Island [*Zhang et al.*, 2008]. This is in agreement with a water mass pathway study on the plateau using radium isotopes during the 2005 KEOPS

cruise, which also found the water mass on the plateau to have originated from Heard Island [*van Beek et al.*, 2008].

We find that the larger bloom event, which extends as far as 100°E in some years, is mostly fertilized by iron advected from Kerguelen Island (see Figure 10), in agreement with *Mongin et al.* [2009] who also performed a modeled advection study on the Kerguelen bloom.

During the recent KEOPS II cruise, iron budgets were calculated focusing on blooms occurring on the plateau, and also offshore in the "plume," which show the importance of a horizontal supply of iron particularly, for the offshore bloom [*Bowie et al.*, 2015]. This separation, in the fertilization of the plateau bloom and offshore bloom, is due to the PF which occurs between the two islands, and flows close to the southern and eastern edge of Kerguelen. Using the definition described in *Park et al.* [2014], the thick black contour in Figure 10 represents the modeled location of the PF for the year 2003. The general position and shape of the PF is fairly consistent each year, however the modeled PF does exhibit small annual variations. In Figure 10, it is apparent that the extent of the Kerguelen Island trajectories, and also in 2003 the bloom, is strongly bounded (in the south) by the location of the PF.

The location of the Crozet bloom was different annually, in some years propagating northwest, but most frequently to the north east of the island. The fertilized patch is also predominately to the north east of Crozet, but there are exceptions in some years when small narrow currents flow northwest from the island. Meridionally, both the fertilized patch and consequently bloom area occur northward of the islands, due to the formation of a Taylor Column around the island vicinity [*Popova et al.*, 2007]. Zonally, the majority of particles are advected by water which has detrained from a branch of the Subantarctic Front (SAF), and are advected eastward which corresponds with the orange Argo float trajectories in *Pollard et al.* [2007, Figure 5]. Lagrangian particles which are advected westward are entrained into a secondary branch from the main SAF, which flows anticyclonic around Del Cano Rise (blue drifter trajectories in *Pollard et al.*, 2007, Figure 5), before eventually turning eastward at roughly 44°. In Figure 6, we see that the years in which the fertilized patch is propagated to the west (2000, 2002, 2003, and 2007), the particle trajectories are from releases earlier in the year, roughly from January to April. This is due to the water mass north of the island (but south of the SAF) being very sluggish, resulting in particle entrainment into the anticyclonic component of the SAF around Del Cano Rise, taking several months.

The model does show potential iron advection extending into all regions of the Crozet annual bloom areas; however, the fertilized patch in the northwest was never as large as the blooms which occurred in the northwest. *Read et al.* [2007] found that submesoscale features were important in the development and duration of the Crozet bloom, and accounted for the bloom's "patchiness." Though the physical model used in this study is at a very high resolution (1/12°), it cannot reproduce the exact eddy field behavior year-on-year, and therefore we do not expect the annual bloom to match the annual fertilized patch. Considering the stochastic nature of eddies, we believe the model to have demonstrated that the local Crozet advection is sufficient to disperse iron into all annual extents of the bloom. Furthermore, the NEMO modeled Lagrangian pathways are in general agreement with drifter data and also altimetry-based Lagrangian model results [*Pollard et al.*, 2007; *Sanial et al.*, 2014].

A bloom associated specifically with iron advected from South Georgia is impossible to delineate in this study, as the surrounding region is one of the most productive areas of the Southern Ocean (Figure. 1a), due to various other sources of iron, e.g., the Antarctic Peninsula [*Ardelan et al.*, 2010; *Murphy et al.*, 2013]. Advection from South Georgia is predominately northward and then eastward, joining with the ACC, overlapping with the annual blooms that occur in the north easterly region of South Georgia [*Korb et al.*, 2004]. There is a striking sloped western edge to both the bloom area and fertilized patch in most years, caused by the position of the PF, which is bounded by the local topography [*Moore et al.*, 1999]. Between South Georgia and the PF and ACC, the modeled advection was annually consistent and likely to fertilize the annually occurring bloom in this area.

4.4. Can Advection Explain the Bloom Inter-Annual Variability?

The area that could potentially be fertilized with iron via advection around Kerguelen annually extends into a fairly consistent spatial coverage, although there are significant inter-seasonal variations. Despite this, the fertilized patch was much larger than the bloom area in all years of the study period, suggesting that

advection alone cannot explain the blooms inter-annual variability. Focusing on 2003, in Figure 10, we see the open ocean bloom extending as far south as 60°S between a southward and then northward deviation of the PF (creating a v shape). However, in most years, the bloom area does not closely match the fertilized patch, and in no years does the bloom propagate as far north (bloom northern limit of 44°S) as the Lagrangian particles. Assuming that the modeled spread of Lagrangian particles is correct, this would suggest that another factor is limiting the spread of the bloom into all areas of available iron, a factor which could be the predominate driver of the inter-annual variability. This would support the theory of silicate limiting the Kerguelen bloom, but without more silicate concentration observations in the far offshore area we can only speculate.

The Crozet blooms during 1998–2007 show a high degree of inter-annual variability, most frequently extending far to the east, but in some years to the west and on occasion extending further north than typical. Our results find a similar degree of inter-annual variability in the modeled local circulation around Crozet, both in the timing of fertilization (i.e., the speed of advection) and the extent of the fertilized patch (i.e., size and direction of patch). Although the fertilized patch in our model does not closely match the observed blooms, our results do suggest that iron advection could predominately control the inter-annual variability seen in the Crozet bloom.

The advection of iron from South Georgia annually covers a similar region (a predominately north, then eastward flow), although there are exceptions. The time scale for fertilization is highly variable (distance traveled from the iron source out into the bloom area per month), which could have an impact on the bloom.

4.5. Factors Controlling Bloom Termination

As the NEMO model offers a range of diagnostics, we can also propose possible bloom termination mechanisms for each island. In the modeled MLD data, the region surrounding Kerguelen does not clearly follow the north to south shallowing of the MLD in summer typical of the Southern Ocean (Figure 9a). There is a very clear divide in the depths of the mixed layer between the shallower north and deeper south at roughly 45°S–50°S. The Kerguelen bloom is always to the south of 45°S, however, in the WOA data set, there is nitrate available north of this, as well as iron according to our advection results (Figure. 5). Additionally, the WOA nitrate concentration is still high in February, so it is unlikely to be nitrate exhaustion that terminates the bloom. We conjecture that as the bloom is constrained to regions with a deep mixed layer, it is dependent on a deep supply of silicate as suggested by *Mongin et al.* [2008], and found to be the case by *Closset et al.* [2014] in the bloom just offshore of the plateau. There is partial evidence from the WOA that the surface silicate concentration downstream of Kerguelen is lower in February, than in the previous 3 months, however, this is based upon very few data. Looking at data from the first KEOPS cruise, Figure 1 in the supplementary material of *Blain et al.* [2007] shows the concentrations of both nitrate and silicate from locations inside and outside of the bloom. It shows that inside the bloom there is no silicate but there is nitrate, whereas outside the bloom there is plenty of both, suggesting silicate to be the limiting nutrient. This suggests that the sampling conducted during the KEOPS II expedition close to the plateau [*Closset et al.*, 2014] needs to be repeated further downstream in future field work in order to determine whether the offshore bloom has similar dynamics longitudinally.

The modeled monthly MLD around the Crozet region does exhibit some inter-annual variability, but typically, shallows north to south from winter into summer, and is shallower than 50 m by the end of the Crozet bloom. However, the WOA climatology suggests that there is still nitrate available in January, which suggests that iron exhaustion most likely terminates the bloom. This is supported by an experiment performed on the CROZEX cruise, where the addition of iron to an area of bloom decline resulted in the stimulation of further phytoplankton growth [*Moore et al.*, 2007].

The South Georgia bloom is the most variable in this study, varying in both timing and extent. The decadal average bloom period is from October to April, although it can last longer and also start earlier in some years. The nitrate concentration remains high throughout the bloom period, which suggests that a deepening mixed layer being the limiting factor for the otherwise persistent South Georgia bloom. This is supported by *Korb et al.* [2008], who found evidence of a persistent supply of both macronutrients and iron, by physical processes, to the area throughout the growing season.

5. Conclusions

In the high-nutrient, low-chlorophyll Southern Ocean [*Martin et al.*, 1990; *de Baar et al.*, 1995; *Boyd et al.*, 2007], blooms are observed in satellite ocean color data occurring annually downstream of Kerguelen, Crozet, and the South Georgia Islands. It is generally accepted that the iron limitation prevailing across the Southern Ocean is locally overcome by the horizontal advection of iron from island sources [*Blain et al.*, 2001; *Murphy et al.*, 2013; *Sanial et al.*, 2014]. In this study, Lagrangian particle tracking, with the NEMO 1/12° ocean general circulation model, was used to assess whether potential iron advection can explain the extent of the blooms, and also their inter-annual variability over the period 1998–2007. We also use the modeled circulation and diagnostic variables to consider possible causes of bloom termination for each of the islands.

We find that lateral advection downstream of the Southern Ocean islands is sufficient to fertilize all areas where annual blooms can occur. The patch fertilized by iron-rich water from Kerguelen is much larger in extent than the area of the bloom, whereas the patch fertilized around Crozet is comparable in size, taking into account inter-annual variability, to the size of the bloom. The patch of water fertilized by iron-rich South Georgia sediments also closely matches with the annual bloom, however, delineating a bloom associated only with South Georgia proved problematic.

The advection around Kerguelen was consistent in spatial extent annually, however, the timing of potential fertilization varied inter-seasonally across the years. This could contribute to the blooms inter-annual variability, however, the results suggest that the far offshore Kerguelen bloom (in some years occurring as far east as 100°E) has another primary factor controlling its inter-annual variability, and we offer the hypothesis of silicate being the ultimate limiting factor on a diatom-dominated Kerguelen bloom. This hypothesis could be tested with in situ nutrient sampling of the area, similar to the recent KEOPS II expedition [*Closset et al.*, 2014], or alternatively by a high-resolution coupled biogeochemical model to properly resolve the key biogeochemical and physical processes. The results suggest that the inter-annual variability seen in the Crozet bloom can be explained by variations in the advected iron supply. The fertilized patch around South Georgia was fairly consistent spatially, however, it did have variations in the timing of advection from the island out to the bloom site. This potentially could account for the inter-annual variability seen in the South Georgia bloom.

In assessing the possible causes of bloom termination, we find that nutrient exhaustion is most likely to cause the Kerguelen and Crozet blooms to collapse (silica and iron, respectively). Whereas winter convection causing the mixed layer to deepen is most likely the terminating factor of the South Georgia bloom, as physical processes maintain a continual supply of macronutrients and iron to the area, these are unlikely to be limiting [*Korb et al.*, 2008]. Typically, both the Kerguelen and Crozet blooms end well before the mixed layer begins to deepen in winter, whereas the South Georgia bloom persists for the entire season until the mixed layer deepens.

References

Abraham, E. R., C. S. Law, P. W. Boyd, S. J. Lavender, M. T. Maldonado, and A. R. Bowie (2000), Importance of stirring in the development of an iron-fertilized phytoplankton bloom, *Nature*, *407*(6805), 727–730, doi:10.1038/35037555.

Ardelan, M. V., O. Holm-Hansen, C. D. Hewes, C. S. Reiss, N. S. Silva, H. Dulaiova, E. Steinnes, and E. Sakshaug (2010), Natural iron enrichment around the Antarctic Peninsula in the Southern Ocean, *Biogeosciences*, *7*(1), 11–25.

Atkinson, A., M. J. Whitehouse, J. Priddle, G. C. Cripps, P. Ward, and M. A. Brandon (2001), The pelagic ecosystem of South Georgia, Antarctica, *Mar. Ecol. Prog. Ser.*, *216*, 279–308.

Aviso (2014), *SSALTO/DUACS User Handbook: (M)SLA and (M)ADT Near–Real Time and Delayed Time Products*, CLS–DOS–NT–06–034, SALP–MU–P–EA–21065–CLS, 59 pp., Cent. Natl. D'études Spatiales, Ramonville St. Agne, France. [Available at http://www.aviso.altimetry.fr/fileadmin/documents/data/tools/hdbk_duacs.pdf.]

Bakker, D. C., M. C. Nielsdottir, P. J. Morris, H. J. Venables, and A. J. Watson (2007), The island mass effect and biological carbon uptake for the subantarctic Crozet Archipelago, *Deep Sea Res., Part II*, *54*, 2174–2190, doi:10.1016/j.dsr2.2007.06.009.

Banse, K. (1996), Low seasonality of low concentrations of surface chlorophyll in the Subantarctic water ring: Underwater irradiance, iron, or grazing?, *Prog. Oceanogr.*, *37*(3-4), 241–291.

Blain, S., et al. (2001), A biogeochemical study of the island mass effect in the context of the iron hypothesis: Kerguelen Islands, Southern Ocean, *Deep Sea Res., Part I*, *48*(1), 163–187, doi:10.1016/S0967-0637(00)00047-9.

Blain, S., et al. (2007), Effect of natural iron fertilization on carbon sequestration in the Southern Ocean, *Nature*, *446*(7139), 1070–1074, doi:10.1038/nature05700.

Blain, S., B. Quéguiner, and T. Trull (2008), The natural iron fertilization experiment KEOPS (KErguelen Ocean and Plateau compared Study): An overview, *Deep Sea Res., Part II*, *55*(5–7), 559–565, doi:10.1016/j.dsr2.2008.01.002.

Blanke, B., and S. Raynaud (1997), Kinematics of the Pacific Equatorial Undercurrent: An Eulerian and Lagrangian approach from GCM results, *J. Phys. Oceanogr.*, *27*(6), 1038–1053, doi:10.1175/1520-0485.

Blanke, B., M. Arhan, G. Madec, and S. Roche (1999), Warm water paths in the equatorial Atlantic as diagnosed with a general circulation model, *J. Phys. Oceanogr.*, *29*, 2753–2768.

Borrione, I., and R. Schlitzer (2013), Distribution and recurrence of phytoplankton blooms around South Georgia, Southern Ocean, *Biogeosciences*, *10*(1), 217–231, doi:10.5194/bg-10-217-2013.

Bowie, A. R., et al. (2015), Iron budgets for three distinct biogeochemical sites around the Kerguelen Archipelago (Southern Ocean) during the natural fertilization study, KEOPS-2, *Biogeosciences*, *12*(14), 4421–4445, doi:10.5194/bg-12-4421-2015.

Boyd, P. W. (2002), Environmental factors controlling phytoplankton processes in the Southern Ocean, *J. Phycol.*, *38*(5), 844–861, doi:10.1046/j.1529-8817.2002.t01-1-01203.x.

Boyd, P. W. (2007), Biogeochemistry: Iron findings, *Nature*, *446*(7139), 989–991, doi:10.1038/446989a.

Boyd, P. W., and M. J. Ellwood (2010), The biogeochemical cycle of iron in the ocean, *Nat. Geosci.*, *3*(10), 675–682, doi:10.1038/ngeo964.

Boyd, P. W., et al. (2000), A mesoscale phytoplankton bloom in the polar Southern Ocean stimulated by iron fertilization, *Nature*, *407*(6805), 695–702, doi:10.1038/35037500.

Boyd, P. W., et al. (2007), Mesoscale iron enrichment experiments 1993–2005: Synthesis and future directions, *Science*, *315*(5812), 612–617, doi:10.1126/science.1131669.

Boyd, P. W., K. R. Arrigo, R. Strzepek, and G. L. van Dijken (2012a), Mapping phytoplankton iron utilization: Insights into Southern Ocean supply mechanisms, *J. Geophys. Res.*, *117*, C06009, doi:10.1029/2011JC007726.

Boyd, P. W., D. C. E. Bakker, and C. Chandler (2012b), A new database to explore the findings from large–scale ocean iron enrichments experiments, *Oceanography*, *25*(4), 64–71, doi:10.5670/oceanog.2012.104.

Boyer, T. P., et al. (2013), World Ocean Database 2013, in *Sydney Levitus*, edited by A. Mishonov, and NOAA Atlas NESDIS 72, 209 pp, doi:10.7289/V5NZ85MT.

Brodeau, L., B. Barnier, A.-M. Treguier, T. Penduff, and S. Gulev (2010) An ERA40-based 461 atmospheric forcing for global ocean circulation models, *Ocean Model.*, *31*, 88–104.

Closset, I., M. Lasbleiz, K. Leblanc, B. Quguiner, A. J. Cavagna, M. Elskens, J. Navez, and D. Cardinal (2014), Seasonal evolution of net and regenerated silica production around a natural Fe-fertilized area in the Southern Ocean estimated with Si isotopic approaches, *Biogeosciences*, *11*(20), 5827–5846, doi:10.5194/bg-11-5827-2014.

Comiso, J. C., C. R. McClain, C. W. Sullivan, J. P. Ryan, and C. L. Leonard (1993), Coastal zone color scanner pigment concentrations in the Southern Ocean and relationships to geophysical surface features, *J. Geophys. Res.*, *98*(C2), 2419–2451, doi:10.1029/92JC02505.

de Baar, H. J., J. T. M. de Jong, D. C. Bakker, B. M. Loscher, C. Veth, U. Bathmann, and V. Smetacek (1995), Importance of iron for plankton blooms and carbon dioxide drawdown in the Southern Ocean, *Nature*, *373*, 412–415, doi:10.1038/373412a0.

de Baar, H. J. W., L. J. A. Gerringa, P. Laan, and K. R. Timmermans (2008), Efficiency of carbon removal per added iron in ocean iron fertilization, *Mar. Ecol. Prog. Ser.*, *364*, 269–282, doi:10.3354/meps07548.

d'Ovidio, F., A. Della Penna, T. W. Trull, F. Nencioli, M. I. Pujol, M. H. Rio, Y. H. Park, C. Cott, M. Zhou, and S. Blain (2015), The biogeochemical structuring role of horizontal stirring: Lagrangian perspectives on iron delivery downstream of the Kerguelen Plateau, *Biogeosciences*, *12*(19), 5567–5581, doi:10.5194/bg-12-5567-2015.

Gille, S. T., M. M. Carranza, and R. Cambra (2014), Wind-induced upwelling in the Kerguelen Plateau region, *Biogeosciences*, *11*(22), 6389–6400, doi:10.5194/bg-11-6389-2014.

Graham, R. M., A. M. De Boer, E. van Sebille, K. E. Kohfeld, and C. Schlosser (2015), Inferring source regions and supply mechanisms of iron in the Southern Ocean from satellite chlorophyll data, *Deep Sea Res., Part I*, *104*, 9–25, doi:10.1016/j.dsr.2015.05.007.

Hewes, C. D., C. S. Reiss, M. Kahru, B. G. Mitchell, and O. Holm–Hansen (2008), Control of phytoplankton biomass by dilution and mixed layer depth in the western Weddell–Scotia Confluence, *Mar. Ecol. Prog. Ser.*, *366*, 15–29, doi:10.3354/meps07515.

Holm-Hansen, O., M. Kahru, and C. D. Hewes (2005), Deep chlorophyll a maxima (DCMs) in pelagic Antarctic waters. II. Relation to bathymetric features and dissolved iron concentrations, *Mar. Ecol. Prog. Ser.*, *297*, 71–81.

Korb, R. E., and M. Whitehouse (2004), Contrasting primary production regimes around South Georgia, Southern Ocean: Large blooms versus high nutrient, low chlorophyll waters, *Deep Sea Res., Part I*, *51*(5), 721–738, doi:10.1016/j.dsr.2004.02.006.

Korb, R. E., M. J. Whitehouse, and P. Ward (2004), SeaWiFS in the southern ocean: Spatial and temporal variability in phytoplankton biomass around South Georgia, *Deep Sea Res., Part II*, *51*, 99–116, doi:10.1016/j.dsr2.2003.04.002.

Korb, R. E., M. Whitehouse, A. Atkinson, and S. E. Thorpe (2008), Magnitude and maintenance of the phytoplankton bloom at South Georgia: A naturally iron-replete environment, *Mar. Ecol. Prog. Ser.*, *368*, 75–91, doi:10.3354/meps07525.

Lasbleiz, M., K. Leblanc, S. Blain, J. Ras, V. Cornet-Barthaux, S. Hlias Nunige, and B. Quguiner (2014), Pigments, elemental composition (C, N, P, and Si), and stoichiometry of particulate matter in the naturally iron fertilized region of Kerguelen in the Southern Ocean, *Biogeosciences*, *11*(20), 5931–5955, doi:10.5194/bg-11-5931-2014.

Le Bars, D., J. V. Durgadoo, H. A. Dijkstra, A. Biastoch, and W. P. M. De Ruijter (2014), An observed 20–year time series of Agulhas leakage, *Ocean Sci.*, *10*(4), 601–609, doi:10.5194/os-10-601-2014.

Madec, G. (2008), NEMO reference manual, ocean dynamic component: NEMO–OPA, Notes du pole de modelisation, *Tech. Rep. 27*, Inst. Pierre Simmon Laplace, Paris.

Martin, J. H., R. M. Gordon, and S. E. Fitzwater (1990), Iron in Antarctic waters, *Nature*, *345*(6271), 156–158, doi:10.1038/345156a0.

Martin, J. M. (1990), Glacial-interglacial CO_2 change: The iron hypothesis, *Paleoceanography*, *5*(1), 1–13.

Marzocchi, A., J. J.-M. Hirschi, N. P. Holliday, S. A. Cunningham, A. T. Blaker, and A. C. Coward (2015), The North Atlantic subpolar circulation in an eddy–resolving global ocean model, *J. Mar. Syst.*, *142*, 126–143, doi:10.1016/j.jmarsys.2014.10.007.

Meredith, M. P., J. L. Watkins, E. J. Murphy, N. J. Cunningham, A. G. Wood, R. Korb, M. J. Whitehouse, S. E. Thorpe, and F. Vivier (2003), An anticyclonic circulation above the Northwest Georgia Rise, Southern Ocean, *Geophys. Res. Lett.*, *30*(20), 2061, doi:10.1029/2003GL018039.

Mongin, M., E. Molina, and T. W. Trull (2008), Seasonality and scale of the Kerguelen plateau phytoplankton bloom: A remote sensing and modeling analysis of the influence of natural iron fertilization in the Southern Ocean, *Deep Sea Res., Part II*, *55*(5–7), 880–892, doi:10.1016/j.dsr2.2007.12.039.

Mongin, M. M., E. R. Abraham, and T. W. Trull (2009), Winter advection of iron can explain the summer phytoplankton bloom that extends 1000 km downstream of the Kerguelen Plateau in the Southern Ocean, *J. Mar. Res.*, *67*, 225–237.

Moore, C. M., S. Seeyave, A. E. Hickman, J. T. Allen, M. I. Lucas, H. Planquette, R. T. Pollard, and A. J. Poulton (2007), Iron–light interactions during the CROZet natural iron bloom and EXport experiment (CROZEX) I: Phytoplankton growth and photophysiology, *Deep Sea Res., Part II*, *54*(18–20), 2045–2065, doi:10.1016/j.dsr2.2007.06.011.

Moore, J. K., and M. R. Abbott (2000), Phytoplankton chlorophyll distributions and primary production in the Southern Ocean, *J. Geophys. Res.*, *105*(C12), 28,709–28,722, doi:10.1029/1999JC000043.

Moore, J. K., M. R. Abbott, and J. G. Richman (1999), Location and dynamics of the Antarctic Polar Front from satellite sea surface temperature data, *J. Geophys. Res.*, *104*(C2), 3059, doi:10.1029/1998JC900032.

Mosseri, J., B. Quguiner, L. Armand, and V. Cornet-Barthaux (2008), Impact of iron on silicon utilization by diatoms in the Southern Ocean: A case study of Si/N cycle decoupling in a naturally iron–enriched area, *Deep Sea Res., Part II*, *55*(5–7), 801–819, doi:10.1016/j.dsr2.2007.12.003.

Murphy, E. J., et al. (2013), Comparison of the structure and function of Southern Ocean regional ecosystems: The Antarctic Peninsula and South Georgia, *J. Mar. Syst.*, *109–110*, 22–42, doi:10.1016/j.jmarsys.2012.03.011.

Orsi, A. H., T. Whitworth III, and W. D. Nowlin Jr. (1995), On the meridional extent and fronts of the Antarctic Circumpolar Current, *Deep Sea Res., Part I*, *42*(5), 641–673.

Park, Y.-H., J.-L. Fuda, I. Durand, and A. C. Naveira Garabato (2008a), Internal tides and vertical mixing over the Kerguelen Plateau, *Deep Sea Res., Part II*, *55* (5-7), 582–593, doi:10.1016/j.dsr2.2007.12.027.

Park, Y.-H., F. Roquet, I. Durand, and J.-L. Fuda (2008b), Large–scale circulation over and around the Northern Kerguelen Plateau, *Deep Sea Res., Part II*, *55*(5–7), 566–581, doi:10.1016/j.dsr2.2007.12.030.

Park, Y.-H., I. Durand, E. Kestenare, G. Rougier, M. Zhou, F. d'Ovidio, C. Cott, and J.-H. Lee (2014), Polar Front around the Kerguelen Islands: An up-to-date determination and associated circulation of surface/subsurface waters, *J. Geophys. Res. Oceans*, *119*, 6575–6592, doi:10.1002/2014JC010061.

Planquette, H., et al. (2007), Dissolved iron in the vicinity of the Crozet Islands, Southern Ocean, *Deep Sea Res., Part II*, *54*, 1999–2019, doi:10.1016/j.dsr2.2007.06.019.

Pollard, R., R. Sanders, M. Lucas, and P. Statham (2007), The Crozet Natural Iron Bloom and Export Experiment (CROZEX), *Deep Sea Res., Part II*, *54*(18–20), 1905–1914, doi:10.1016/j.dsr2.2007.07.023.

Pollard, R. T., H. J. Venables, J. F. Read, and J. T. Allen (2007), Large–scale circulation around the Crozet Plateau controls an annual phytoplankton bloom in the Crozet Basin, *Deep Sea Res., Part II*, *54*, 1915–1929, doi:10.1016/j.dsr2.2007.06.012.

Pollard, R. T., et al. (2009), Southern Ocean deep-water carbon export enhanced by natural iron fertilization, *Nature*, *457*(7229), 577–580, doi:10.1038/nature07716.

Popova, E. E., R. T. Pollard, M. I. Lucas, H. J. Venables, and T. R. Anderson (2007), Real-time forecasting of ecosystem dynamics during the CROZEX experiment and the roles of light, iron, silicate, and circulation, *Deep Sea Res., Part II*, *54*(18-20), 1966–1988, doi:10.1016/j.dsr2.2007.06.018.

Popova, E. E., A. Yool, Y. Aksenov, and A. C. Coward (2013), Role of advection in Arctic Ocean lower trophic dynamics: A modeling perspective, *J. Geophys. Res. Oceans*, *118*, 1571–1586, doi:10.1002/jgrc.20126.

Poulton, A. J., C. Mark Moore, S. Seeyave, M. I. Lucas, S. Fielding, and P. Ward (2007), Phytoplankton community composition around the Crozet Plateau, with emphasis on diatoms and Phaeocystis, *Deep Sea Res., Part II*, *54*(18-20), 2085–2105, doi:10.1016/j.dsr2.2007.06.005.

Read, J. F., R. T. Pollard, and J. T. Allen (2007), Sub–mesoscale structure and the development of an eddy in the Subantarctic Front north of the Crozet Islands, *Deep Sea Res., Part II*, *54*(18–20), 1930–1948, doi:10.1016/j.dsr2.2007.06.013.

Robinson, J., E. E. Popova, A. Yool, M. Srokosz, R. S. Lampitt, and J. R. Blundell (2014), How deep is deep enough? Ocean iron fertilization and carbon sequestration in the Southern Ocean, *Geophys. Res. Lett.*, *41*, 2489–2495, doi:10.1002/2013GL058799.

Sanial, V., P. van Beek, B. Lansard, F. d'Ovidio, E. Kestenare, M. Souhaut, M. Zhou, and S. Blain (2014), Study of the phytoplankton plume dynamics off the Crozet Islands (Southern Ocean): A geochemical-physical coupled approach, *J. Geophys. Res. Oceans*, *119*, 2227–2237, doi:10.1002/2013JC009305.

Schallenberg, C., P. van der Merwe, F. Chever, J. T. Cullen, D. Lannuzel, and A. R. Bowie (2016), Dissolved iron and iron(II) distributions beneath the pack ice in the East Antarctic (120°E) during the winter/spring transition, *Deep Sea Res., Part II*, doi:10.1016/j.dsr2.2015.02.019, in press.

Shaked, Y., and H. Lis (2012), Disassembling iron availability to phytoplankton, *Frontiers Microbiol.*, *3*(123), 1–26, doi:10.3389/fmicb.2012.00123.

Smetacek, V., P. Assmy, and J. Henjes (2004), The role of grazing in structuring Southern Ocean pelagic ecosystems and biogeochemical cycles, *Antarct. Sci.*, *16*(4), 541–558, doi:10.1017/S0954102004002317.

Srokosz, M. A., J. Robinson, H. McGrain, E. E. Popova, and A. Yool (2015), Could the Madagascar bloom be fertilized by Madagascan iron?, *J. Geophys. Res. Oceans*, *120*, 5790–5803, doi:10.1002/2015JC011075.

Storm, T., M. Boettcher, M. Grant, M. Zuhlke, N. Fomferra, T. Jackson, and S. Sathyendranath (2013), Product user guide, in *Ocean Colour Climate Change Initiative (OC_CCI)—Phase One*, edited by S. Groom, Plymouth Mar. Lab., 14 pp., Plymouth, U. K.

Tagliabue, A., J.-B. Salle, A. R. Bowie, M. Lvy, S. Swart, and P. W. Boyd (2014), Surface-water iron supplies in the Southern Ocean sustained by deep winter mixing, *Nat. Geosci.*, *7*(4), 314–320, doi:10.1038/ngeo2101.

Takahashi, T., et al. (2009), Climatological mean and decadal change in surface ocean pCO_2, and net sea–air CO_2 flux over the global oceans, *Deep Sea Res., Part II*, *56*(8-10), 554–577, doi:10.1016/j.dsr2.2008.12.009.

Thomalla, S. J., N. Fauchereau, S. Swart, and P. M. S. Monteiro (2011), Regional scale characteristics of the seasonal cycle of chlorophyll in the Southern Ocean, *Biogeosciences*, *8*(10), 2849–2866, doi:10.5194/bg-8-2849-2011.

Tripathy, S. C., S. Pavithran, P. Sabu, H. U. K. Pillai, D. R. G. Dessai, and N. Anilkumar (2015), Deep chlorophyll maximum and primary productivity in Indian Ocean sector of the Southern Ocean: Case study in the Subtropical and Polar Front during austral summer 2011, *Deep Sea Res., Part II*, *118*, 240–249, doi:10.1016/j.dsr2.2015.01.004.

Tyrrell, T., A. Merico, J. J. Waniek, C. S. Wong, N. Metzl, and F. Whitney (2005), Effect of seafloor depth on phytoplankton blooms in high-nitrate, low-chlorophyll (HNLC) regions, *J. Geophys. Res.*, *110*, G02007, doi:10.1029/2005JG000041.

van Beek, P., M. Bourquin, J. L. Reyss, M. Souhaut, M. A. Charette, and C. Jeandel (2008), Radium isotopes to investigate the water mass pathways on the Kerguelen Plateau (Southern Ocean), *Deep Sea Res., Part II*, *55*(5–7), 622–637, doi:10.1016/j.dsr2.2007.12.025.

van der Merwe, P., et al. (2015), Sourcing the iron in the naturally fertilised bloom around the Kerguelen Plateau: Particulate trace metal dynamics, *Biogeosciences*, *12*(3), 739–755, doi:10.5194/bg-12-739-2015.

Venables, H., and C. M. Moore (2010), Phytoplankton and light limitation in the Southern Ocean: Learning from high-nutrient, high-chlorophyll areas, *J. Geophys. Res.*, *115*, C02015, doi:10.1029/2009JC005361.

Venables, H. J., R. T. Pollard, and E. E. Popova (2007), Physical conditions controlling the development of a regular phytoplankton bloom north of the Crozet Plateau, Southern Ocean, *Deep Sea Res., Part II*, *54*, 1949–1965, doi:10.1016/j.dsr2.2007.06.014.

Wadley, M. R., T. D. Jickells, and K. J. Heywood (2014), The role of iron sources and transport for Southern Ocean productivity, *Deep Sea Res., Part I*, *87*, 82–94, doi:10.1016/j.dsr.2014.02.003.

Ward, P., M. Whitehouse, R. Shreeve, S. Thorpe, A. Atkinson, R. Korb, D. Pond, and E. Young (2007), Plankton community structure south and west of South Georgia (Southern Ocean): Links with production and physical forcing, *Deep Sea Res., Part I*, *54*, 1871–1889, doi: 10.1016/j.dsr.2007.08.008.

Young, E. F., M. P. Meredith, E. J. Murphy, and G. R. Carvalho (2011), High-resolution modelling of the shelf and open ocean adjacent to South Georgia, Southern Ocean, *Deep Sea Res., Part II*, *58*, 1540–1552, doi:10.1016/j.dsr2.2009.11.003.

Young, E. F., S. E. Thorpe, N. Banglawala, and E. J. Murphy (2014), Variability in transport pathways on and around the South Georgia shelf, Southern Ocean: Implications for recruitment and retention, *J. Geophys. Res. Oceans*, *119*, 241–252, doi:10.1002/2013JC009348.

Zhang, Y., F. Lacan, and C. Jeandel (2008), Dissolved rare earth elements tracing lithogenic inputs over the Kerguelen Plateau (Southern Ocean), *Deep Sea Res., Part II*, *55*, 638–652, doi:10.1016/j.dsr2.2007.12.029.